Calibration of the CHARM Fine-Grained Calorimeter

CHARM Collaboration

J.Dorenbosch and F.Udo
NIKHEF, Amsterdam, The Netherlands

J.V.Allaby, U.Amaldi, G.Barbiellini[1], F.Bergsma, A.Capone[2], W.Flegel,
L.Lanceri, M.Metcalf, C.Nieuwenhuis, J.Panman, C.Santoni[3] and K. Winter
CERN, Geneva, Switzerland

I.Abt, J.Aspiazu, A.Büngener, F.W.Büsser, H.Daumann,
P.D.Gall, T.Hebbeker, F.Niebergall, P.Schütt, and P.Stähelin
II. Institut für Experimentalphysik[4], Universität Hamburg, Hamburg, Germany

P.Gorbunov, E.Grigoriev, V.Khovansky and A.Rosanov
Institute for Theoretical and Experimental Physics, Moscow, USSR

A.Baroncelli[5], L.Barone[6], B.Borgia[6], C.Bosio[5], M.Diemoz[6],
U.Dore[6], F.Ferroni[6], E.Longo[6], L.Luminari[6], P.Monacelli[6],
S.Morganti[6], F.de Notaristefani[6], L.Tortora[5] and V.Valente[7]
Istituto Nazionale di Fisica Nucleare, Rome, Italy

(Submitted to Nuclear Instruments and Methods)

Abstract

Calorimeters have been used extensively for the study of neutrino interactions in the last decade. This paper describes the need for calibration of such calorimeters and how this was realized for the case of the CHARM fine-grained calorimeter. The energy and spatial response of the calorimeter to both hadronic and electromagnetic showers was measured in π and electron beams from 5 to 140 GeV. The results and resolutions are presented.

[1] On leave of absence from INFN, LN Frascati, Italy.

[2] On leave of absence from Università "La Sapienza", Rome, Italy.

[3] On leave of absence from INFN Sezione Sanità and Istituto Superiore di Sanità, Rome, Italy.

[4] Supported by Bundesministerium für Forschung und Technologie, Bonn, German Fed. Republic.

[5] INFN Sezione Sanità and Istituto Superiore di Sanità, Rome, Italy.

[6] Dipartimento di Fisica, Università "La Sapienza", Roma and INFN Sezione di Roma, Rome, Italy.

[7] Laboratori Nazionali INFN Frascati, Italy.

Contents

Tables

Figures

1. Introduction

1.1 Calorimetry in Neutrino Experiments

The neutrino (or its anti-particle the antineutrino), can justly be described as the most elusive of the fundamental particles. This quality stems from the lack of properties which could lead to easy detection. The neutrino has no electric charge and, to the best of our current knowledge, has no intrinsic mass. The lack of electric charge means that a neutrino will pass through matter without causing ionisation and will pass through electric or magnetic fields without suffering any deflection. The lack of intrinsic mass constrains the neutrino to travel always at the velocity of light. Furthermore, as far as we know, neutrinos are completely stable and do not decay into other particles which might be easier to detect.

Hence, the only way that the presence of neutrinos can be detected (rather than inferred) is through their interaction, and even this is extremely weak. For example, the probability that a neutrino of 4 GeV energy will interact with a given target is 10^{-12} that with which a proton would interact with the same target.

Despite these inherent difficulties, ever since the existence of accelerators of sufficient energy (such as the proton synchrotrons of energy greater than 10 GeV), beams of neutrinos have been produced and experiments have been carried out using these beams.

The detectors of neutrinos, which must rely on producing interactions of these elusive particles, have necessarily been massive in order to produce a significant number of interactions in a finite time. These have been of two types. Large bubble chambers, usually containing several tons of liquid, in which the rare neutrino events have been detected by photographing the ionisation tracks produced by the charged products of the neutrino interactions. The second type of detector has been developed in order to use the maximum amount of material and thus to produce large numbers of neutrino interactions for detailed study. It comprises typically laminations of solid material interspersed with detector layers which record signals proportional to the number of charged tracks which have passed through each layer, thus "sampling" the deposition of energy of the hadronic shower produced by the neutrino interaction. This type of detector has become known as the target calorimeter, since it acts both as a massive target to produce neutrino interactions, and as an energy detector to measure the amount of energy released by the neutrino interaction. Such detectors have masses of several hundred tons, and have yielded hundreds of thousands of neutrino events.

These two types of detectors have played a complementary role in neutrino physics in the last two decades; the bubble chamber giving extremely fine resolution of the charged tracks produced in neutrino interactions, whilst the target calorimeter detectors have yielded many more interactions in which much less detail of the final state could be seen. It is natural that both these kinds of detector have evolved with time. The bubble chamber detectors have added muon detectors outside the chamber itself in order to improve the efficiency for detection of the high-energy muons produced commonly in neutrino interactions (in the so-called charged-current reactions of muon-neutrinos ν_μ). The target calorimeters have become more and more sophisticated in an attempt to measure more than just the energy of the hadronic shower and the direction of the outgoing muon, when present.

With the increasing sophistication of target calorimeters has come an even greater need for sophisticated calibration of their response. This paper will deal with the methods used to calibrate the response of a fine-grained target calorimeter used by the CHARM Collaboration [1] in a series of neutrino experiments over the period 1977-1984 in which not only the reaction energy was measured, but also the direction and composition of the hadronic shower as well as the momentum of the outgoing muon produced in charged current reactions. The results of a first calibration of the detector, appropriate to the early phase of its existence, have been published [2] previously.

1.2 The Need for Calibration of Calorimeters

In any neutrino experiment, the knowledge of the amount of energy deposited by the interacting neutrino is important. For example, in the study of charged-current interactions of neutrinos on nuclei, the measured shower energy can be equated with the energy of the produced hadrons, E_H, which may be simply added to the energy of the muon to yield the incident neutrino energy, E_ν, as well as yielding the inelasticity of the event (from the ratio $y = E_H/E_\nu$). In the case of neutral-current interactions on nuclei, where the emerging lepton is no longer a muon, but an unseen neutrino, the hadron energy and the lateral position of the interaction vertex must be known in order to deduce the energy of the incoming neutrino from a knowledge of the momentum of the parent π or K in the beam.

In both these examples, it is necessary to know how to convert the detector response, usually based on a sum of pulse-heights from the active planes of the calorimeter, into a real energy in GeV, including the resolution with which this can be achieved.

Since, as will be shown later, the techniques of calibration involve the exposure of the detector to beams of charged particles, it is also necessary to provide some way to keep track of changes in the detector response on a continuous basis, since exposure of the detector to such charged particle beams necessarily occurs rather infrequently. This is commonly done by continuously recording the response of the detector to the passage of cosmic-ray muons, which are minimum ionizing particles in the case of large calorimeters with appropriate triggering. This can be carried out throughout the exposure of the calorimeter to the neutrino beam during the time in between the bursts of neutrinos produced by the accelerator. After correction for the angle of incidence of the muons with respect to the detector planes, the pulse-height response of the detector can be converted into an equivalent number of minimum ionizing particles passing normally through a detector plane.

Thus a calibration of the energy response of a target calorimeter involves comparing the output of the detector planes when exposed to a beam of charged particles of known energy with the output of the same detector from events initiated by cosmic-ray muons and recorded at the same time (i.e. between accelerator bursts). The output of the detector from a charged particle of known energy can thus be interpreted as an equivalent number of minimum ionizing particles.

Under neutrino exposure conditions, the response of the detector to neutrino-induced showers can then be converted into the energy of a charged particle which would produce the equivalent output, using the intermediate step of conversion to minimum ionizing response to eliminate drifts between calibration periods.

As remarked already, in order to deduce the incident neutrino energy from the observed shower energy in neutral-current reactions, the lateral position of the interaction vertex is needed to define the decay kinematics of the parent π or K. Calibration of the precision with which the shower vertex can be determined is thus needed.

In the specific case of the CHARM fine-grain calorimeter, the use of spatial information extends even further. This calorimeter has been used to measure neutral-current interactions where the only source of information on the kinematics of the final state of the neutrino interaction is the hadronic shower. Not only the shower energy and vertex, but also the energy-flow vector of the shower was measured. Calibration of the resolution with which this vector could be measured was clearly necessary in order to unfold the desired kinematic variables from the observed data. This type of information can also be obtained by exposing the calorimeter to charged particle beams where the trajectory of the incident particles is recorded together with the calorimeter data.

1.3 Use of Pion and Electron Beams - Shower Development

The response of calorimeters to hadronic and electromagnetic showers is in general not identical. Hence calibration must be carried out with beams of hadrons (usually π^-) and with beams of electrons. When the neutrino-induced shower contains both electrons and hadrons, as occurs in the case of the interaction of electron neutrinos, special techniques are necessary to recognize the electromagnetic shower amongst the hadronic components (see section 3.6).

It is assumed in all calibration work on calorimeters operating above about 1 GeV that the energy deposition of a neutrino-induced hadronic shower is insignificantly different from that produced by a single π of the same energy. This assumption is equivalent to assuming that a constant energy-independent fraction of the deposited energy is detected. Thus by exposing the detector (or at least a sufficiently large fraction of it) to pion beams of different energies one can create a calibration curve which will relate the detector output to a true energy in GeV.
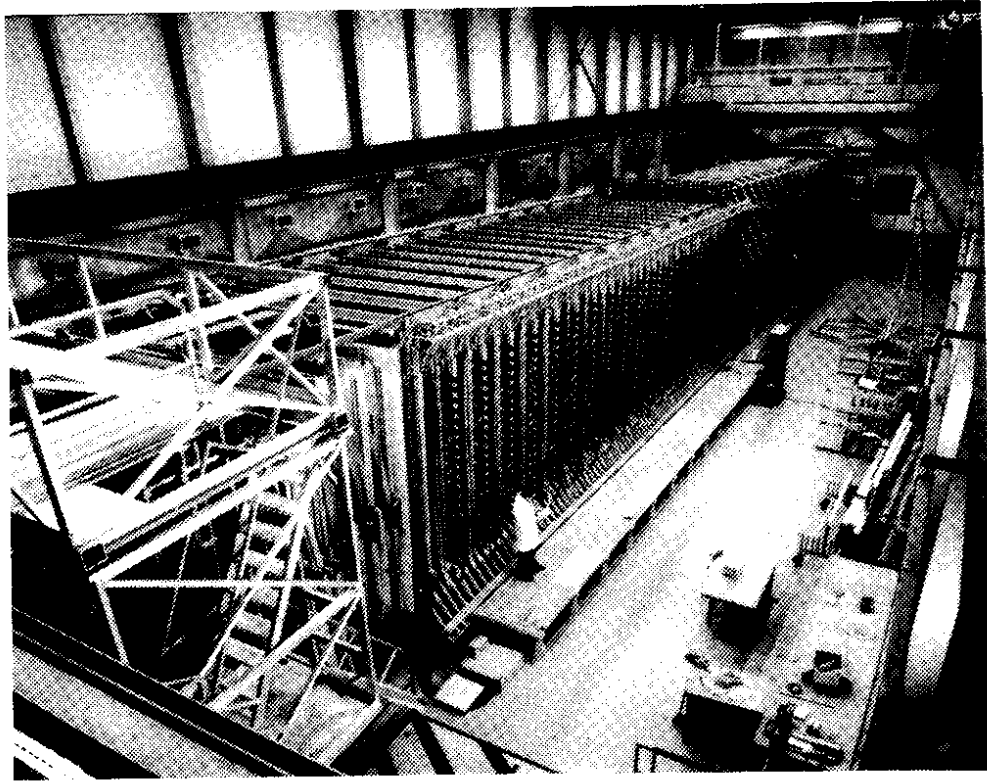
Figure 1: Photograph of the CHARM Calorimeter.

Care must be taken that only pions are used for the calibration, and for this purpose a Cherenkov counter in the beam is required which can positively identify the incident particle as a pion. To simplify this task, π^- beams are preferred because they are naturally richer in pions than the corresponding positive beams. At high energies where it is difficult to separate electrons from pions by Cherenkov techniques, the electrons are removed by inserting a thin layer of lead in the beam-line upstream of the last bending magnet in front of the detector. Contamination of the sample of events by beam muons must be eliminated at the analysis stage, since these particles do not produce showers, and deposit far less energy in the calorimeter.

Calibration of the detector energy response to electrons is done in a similar manner. Again a Cherenkov counter can be used to identify electrons in a mixed beam.

In order to fully study the spatial resolution, the charged particle beam must be well measured before it enters the calorimeter, so that the lateral vertex position of the shower is known from the incoming vector of the charged particle. In the case of electron beams, care must be taken to eliminate those events where the electron initiated a shower before entering the calorimeter, which would falsify the measurements of the shower vertex.

In the case of the CHARM calorimeter, where the energy flow vector was measured, the response of the detector to charged particles incident at different angles needed to be calibrated so the test beam had to have that possibility over a reasonable angular range.

2. The CHARM Calorimeter

2.1 Components of the Calorimeter

The neutrino detector used by the CERN-Hamburg-Amsterdam-Rome-Moscow Collaboration, consists of a fine-grained target calorimeter, here referred to as the CHARM calorimeter, composed of 78 identical subunits, each surrounded by a frame of magnetized iron for muon identification, and of a muon spectrometer. It has been described in detail [1] previously. A photograph of this detector is shown in Figure 1.

Each subunit comprises the following elements (see Figure 2):

- A marble ($CaCO_3$) plate, 3×3 m^2 in surface area and 8 cm thick, surrounded by a magnetized iron frame of the same thickness and 45 cm wide.
- An array of 20 scintillation counters, each of 3 m length, 15 cm width and 3 cm thickness, covering the surface of the marble plate.
- An array of 128 proportional drift tubes, each of 3×3 cm^2 cross-section and 4 m length, covering the surface of the marble plate and the surrounding iron frame. The proportional tubes were oriented at $90°$ with respect to the scintillation counters.
- An array of 256 limited streamer tubes, each of 1×1 cm^2 cross-section and forming a plane of about 2.65×2.65 m^2 sensitive area, covering the centre-most region of the marble plate. The streamer tubes were oriented at $90°$ with respect to the proportional tubes (i.e. parallel to the scintillation counters). The streamer tube planes [4] were added to the detector in 1980 to improve the vertex determination, by allowing accurate lateral track sampling in two orthogonal projections in each subunit.

The marble plates, each weighing 2 tons, formed the target material for the neutrino interactions and was the principal radiator material of the calorimeter. The choice of this material was made, following extensive Monte Carlo simulation, in order to minimize the difference in length of hadronic and electromagnetic showers of the same energy, so that hadronic showers with abnormal π^0 content would not degrade the angular resolution of the measurement of the energy-flow vector. Aluminium

Figure 2: Partial View of the CHARM Calorimeter.
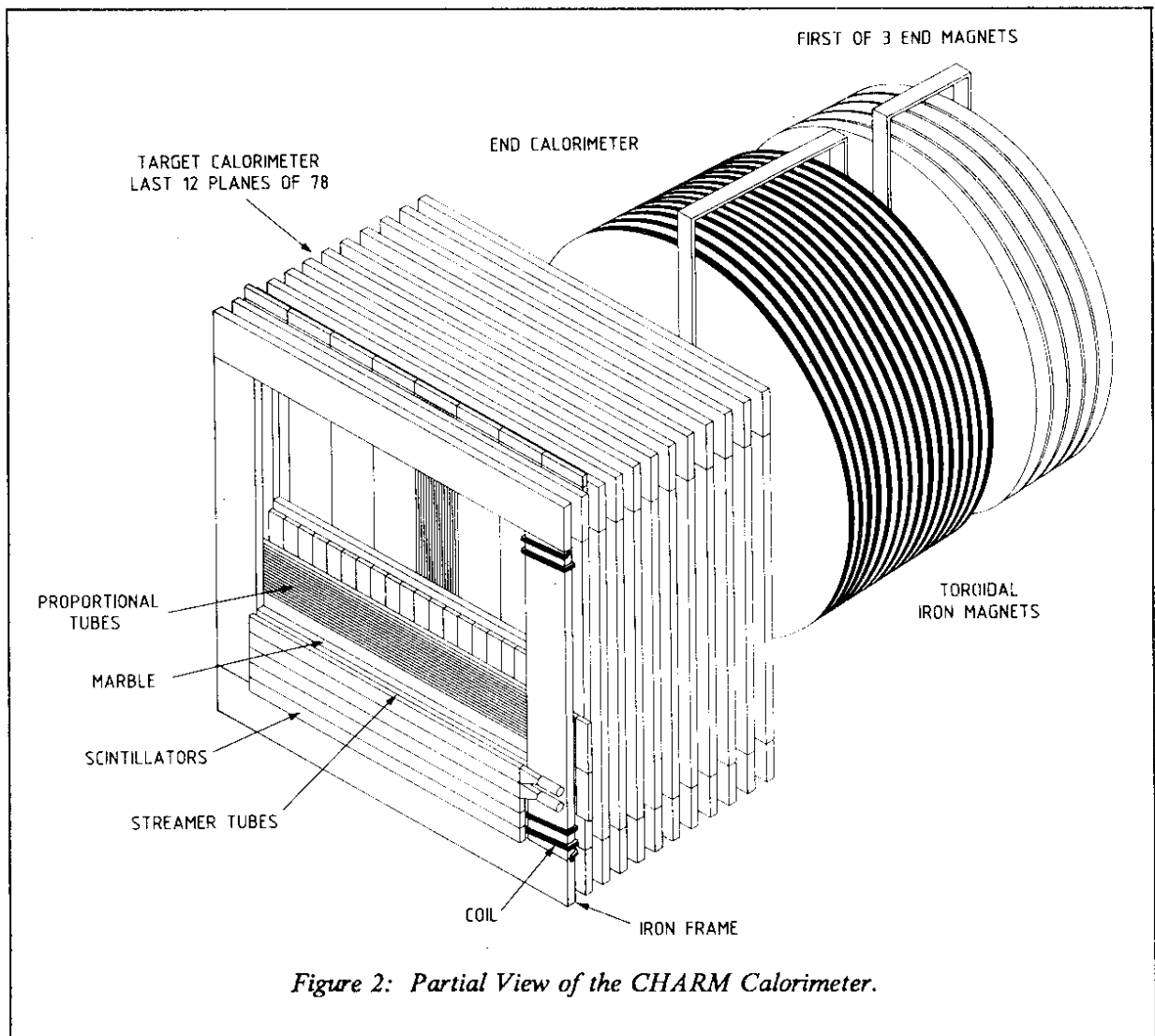
could also have been used, since its physical properties (radiation length, absorption length, density) are similar to marble, but would have been much more expensive.

2.2 The Scintillator System

The scintillation counters had two very important functions. They were the elements used to trigger the detector and initiate the readout of the other components. They were also the principal and most precise detector of the energy deposited by a shower.

The scintillation counters, each 3m long, were coupled at one end by light-pipes to a photomultiplier tube. The other end of each scintillator was terminated with a plane mirror to minimize the variation in pulse-height response with the position at which the particles traversed the scintillator. The orientation of the scintillators was such that the photomultiplier tubes appeared (as seen from the beam direction) sequentially up, right, down, left with respect to the calorimeter. In this way, the response of the scintillators to tracks penetrating at least four planes was made essentially independent of the location of the track.

Figure 3: Differential Trigger Inefficiency vs Hadron Energy
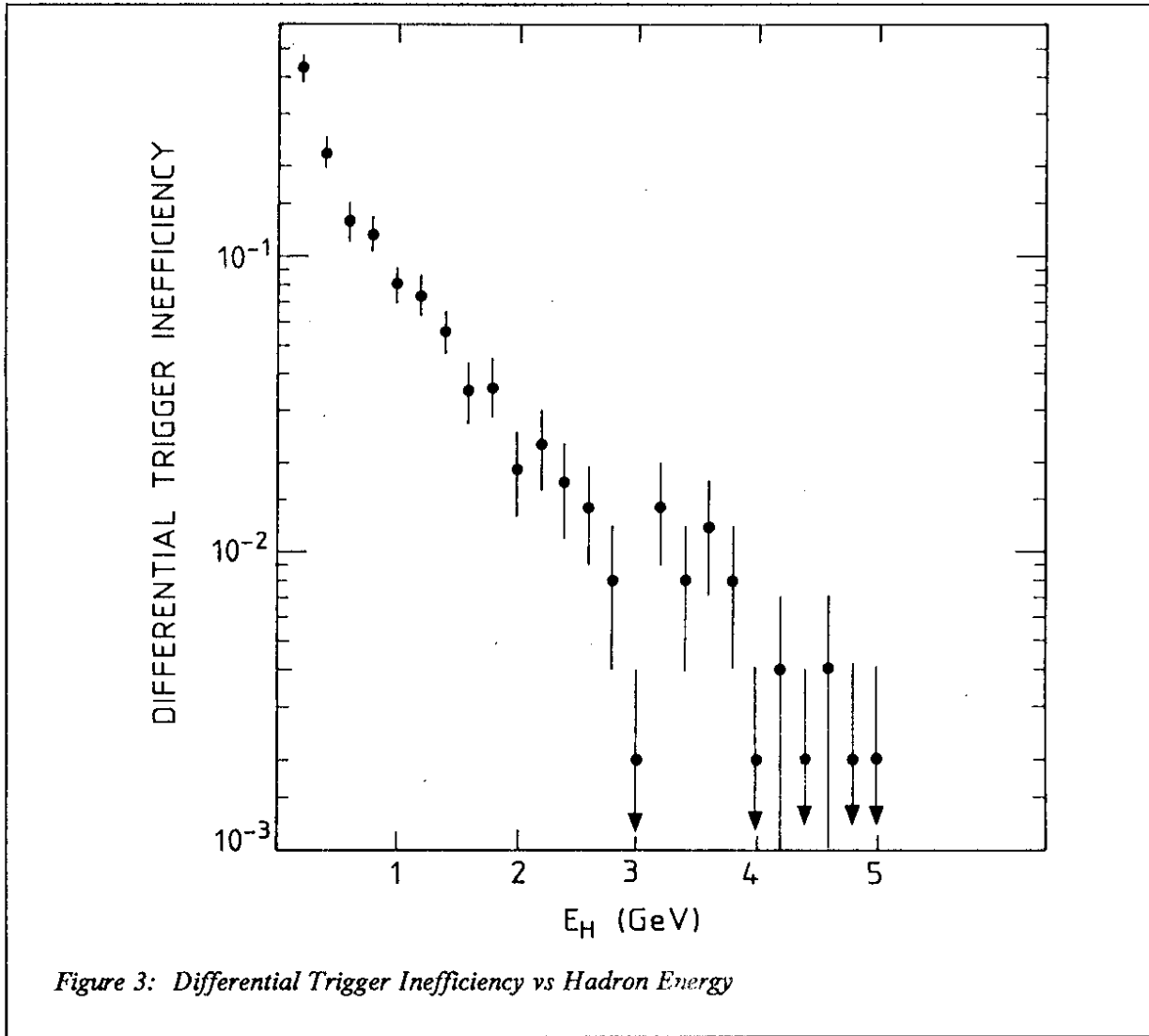
The most inclusive trigger used with the CHARM calorimeter for neutrino detection at high energies required that hits were detected in any 4 of the 78 planes of scintillators. This trigger was measured to have an integral inefficiency of $(6.2 \pm 0.7).10^{-4}$ for $E_H > 2$ GeV. The differential inefficiency for this trigger as a function of the measured energy deposition is shown in Figure 3.

Other triggers used during the various experiments performed with the CHARM calorimeter required that the pulse-height sum from the scintillators exceeded a given threshold or that a track penetrated a greater number of planes. For example, the trigger used outside the time of the beam burst to record cosmic-ray muons for calibration purposes required penetration through the equivalent of 12 planes of the calorimeter. This was necessary in order to eliminate very steep muon tracks which would pass through the scintillators with grazing angles of incidence producing very large energy deposit.

As a result of the sequential orientation of the scintillators, no attenuation correction was needed for the individual charged tracks of showers in the calorimeter. Nevertheless, attenuation corrections were applied to each scintillator output based on the position of the barycentre of the shower in each scintillator plane, as measured by the proportional tubes. Attenuation corrections were also needed for

the calibration of the scintillator output in terms of the equivalent number of minimum ionizing particles traversing a single scintillator plane.

The light attenuation properties of each scintillation counter were measured before installation in the calorimeter. The response of the scintillators as a function of the distance x from the light-guide could be represented analytically by the formula:

$$f(x) = K[\exp(-x/\lambda) + \rho\exp(x-2L)/\lambda]$$

where K is a constant, ρ a reflectivity coefficient ≈ 0.8, λ the attenuation length, and L its physical length.

During the course of the experiments using the calorimeter, cosmic-ray data were taken at intervals of about two months specifically to measure the light attenuation properties. About 500,000 tracks through the calorimeter were recorded on each occasion. These tracks were reconstructed in space using the proportional tube information (see next section) so that the point of intersection of the muon track with each scintillator and its angle of incidence were known. The pulse-height response of each scintillator was corrected to yield the output which a muon of normal incidence would have produced. The corrected response of each scintillator was then histogrammed in bins of 10cm along its length, and the shape of the histogram was fitted using the function f(x) given above, or more usually an approximation of it by a second-order polynomial which gave better values of χ^2. The fit was made excluding the two end bins where edge effects cause deviations from the simple functional form used. The deviations of the two end bins were explicitly taken into account. The difference between the measured transmission and the fit is shown in Figure 4.

It was found that the light transmission properties of the scintillator showed a degradation with time and in particular, the absorption length, λ, decreased at a rate of $\approx 1.5\%$ per month. Measurements showed that the principal degradation occurred for the shorter wavelengths, so corrective action was taken in 1980, at the time when the streamer tubes were added to the calorimeter, by inserting yellow filters in front of each photomultiplier. This restored the original attenuation length, at the cost of a factor two in photomultiplier output, but did not remove totally the dependence of λ on time, although it became less serious (0.63% per month).

In addition to these special attenuation measurements, cosmic-ray muons were recorded continuously during data taking in between the bursts of neutrinos. The tracks of these events were fitted as described above and used to provide a calibration of the pulse-height output of the scintillators in terms of an equivalent number of minimum ionizing particles traversing the standard thickness of scintillator, after correcting for the angle of incidence of each muon track, and the attenuation of each counter. The uniformity of this calibration procedure over the whole detector, ensuring equal mean energy loss, was carefully checked and found to be realized to within $\pm$ 0.5%.

This calibration procedure ensured that the output of the scintillation counters was converted into a physical quantity measured with the same apparatus at the same time, and thus eliminated drifts in gain of the photomultipliers and changes in the properties of the analogue-to-digital converters, as well as the slow changes in the properties of the scintillators themselves. The uncertainty of this procedure has been estimated to be $\pm$ 2%.

The scintillator output provided a definition of the longitudinal position of the shower vertex which was taken as the centre of the marble plate behind which an energy loss corresponding to more than the equivalent of four minimum ionizing particles was detected in two contiguous scintillator planes. The barycentre of the energy deposition in the scintillators (after subtracting the energy deposited by the muon track, if present) was used as the first estimate of the centre of the shower, and the line joining this point to the vertex gave an estimate of the shower direction.

Figure 4: Scintillator Response: Deviation from Parabolic Fit
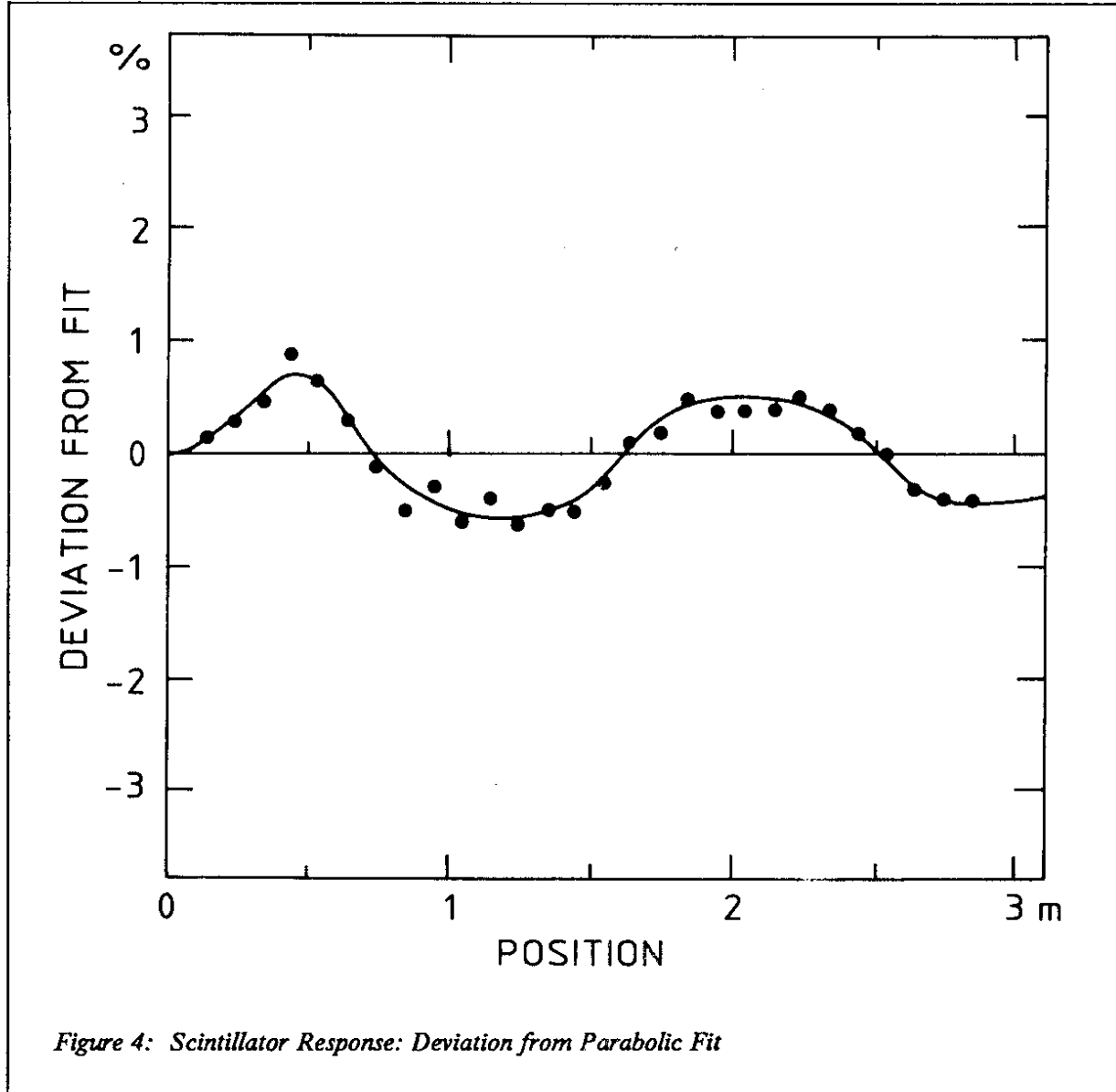
2.3 Proportional Drift Tube System

The proportional tubes of the CHARM calorimeter (78 layers in the target calorimeter and 18 layers in the muon spectrometer) were required to locate muon tracks with a precision of < 1 mm. In addition, the energy of particle showers was sampled by these planes in the same way as done with the scintillators. However, the proportional tube planes in the target calorimeter covered an area of 4×4 m^2 and thus could be used to sample the energy "leaking" into the iron frame surrounding the marble plates. The proportional tube planes in the first iron toroid of the muon spectrometer could also sample the energy leakage from the end of the target calorimeter.

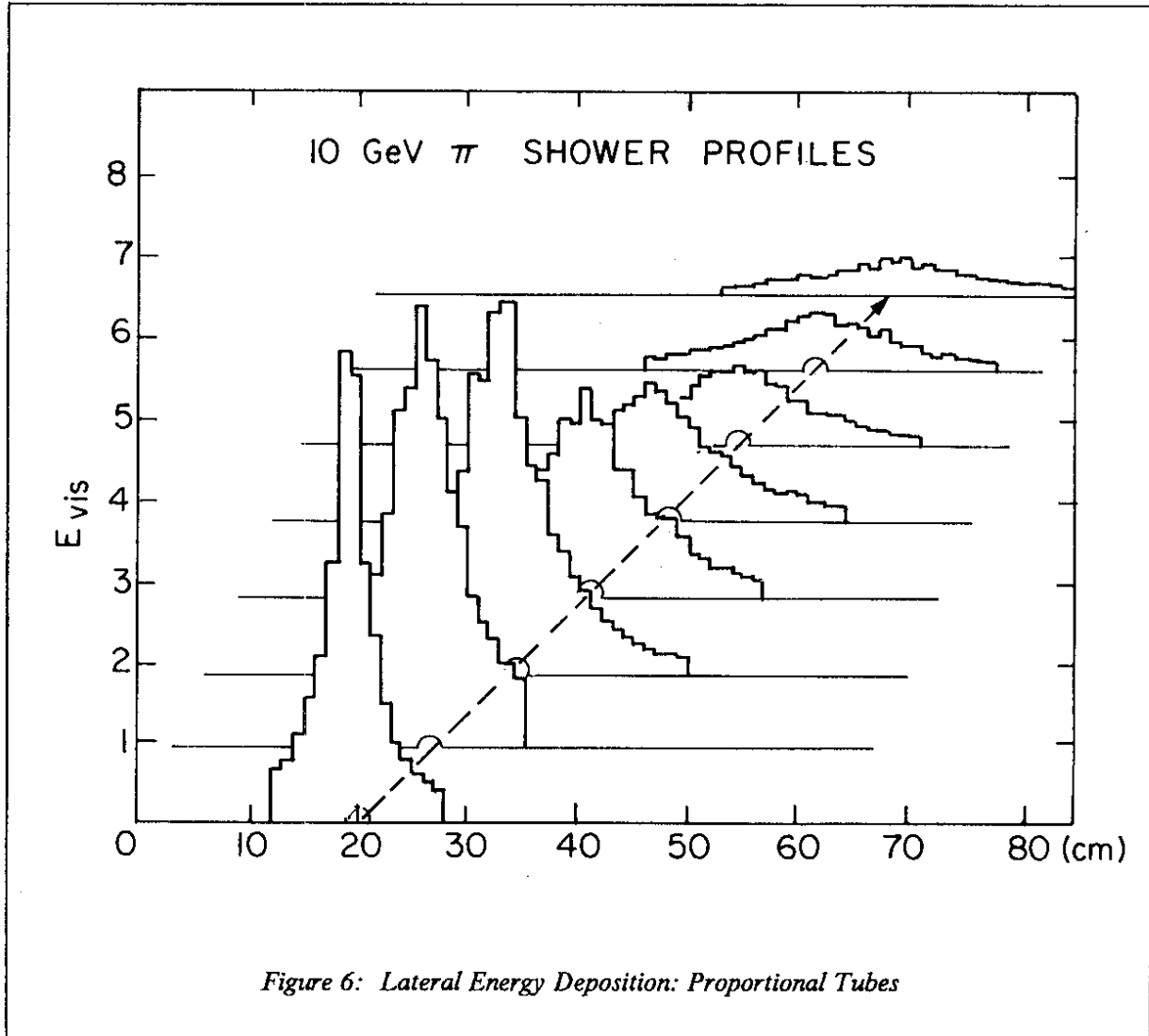Each wire of the proportional tubes was connected to a charge amplifier. Self-triggering electronics provided measurements of the charge and the time-of-arrival of the pulse from each wire. An external gate signal, derived from the scintillation counter trigger, enabled the electronics for charge measurement and set the time reference for the drift-time measurement. The drift-time was calibrated using

high-energy muons and the calibration curve is shown in Figure 5. In order to solve the left-right am-
biguity, consecutive planes of the same orientation were aligned staggered by one-half of the wire
spacing.

Figure 5: Drift-Time Calibration: Proportional Tubes
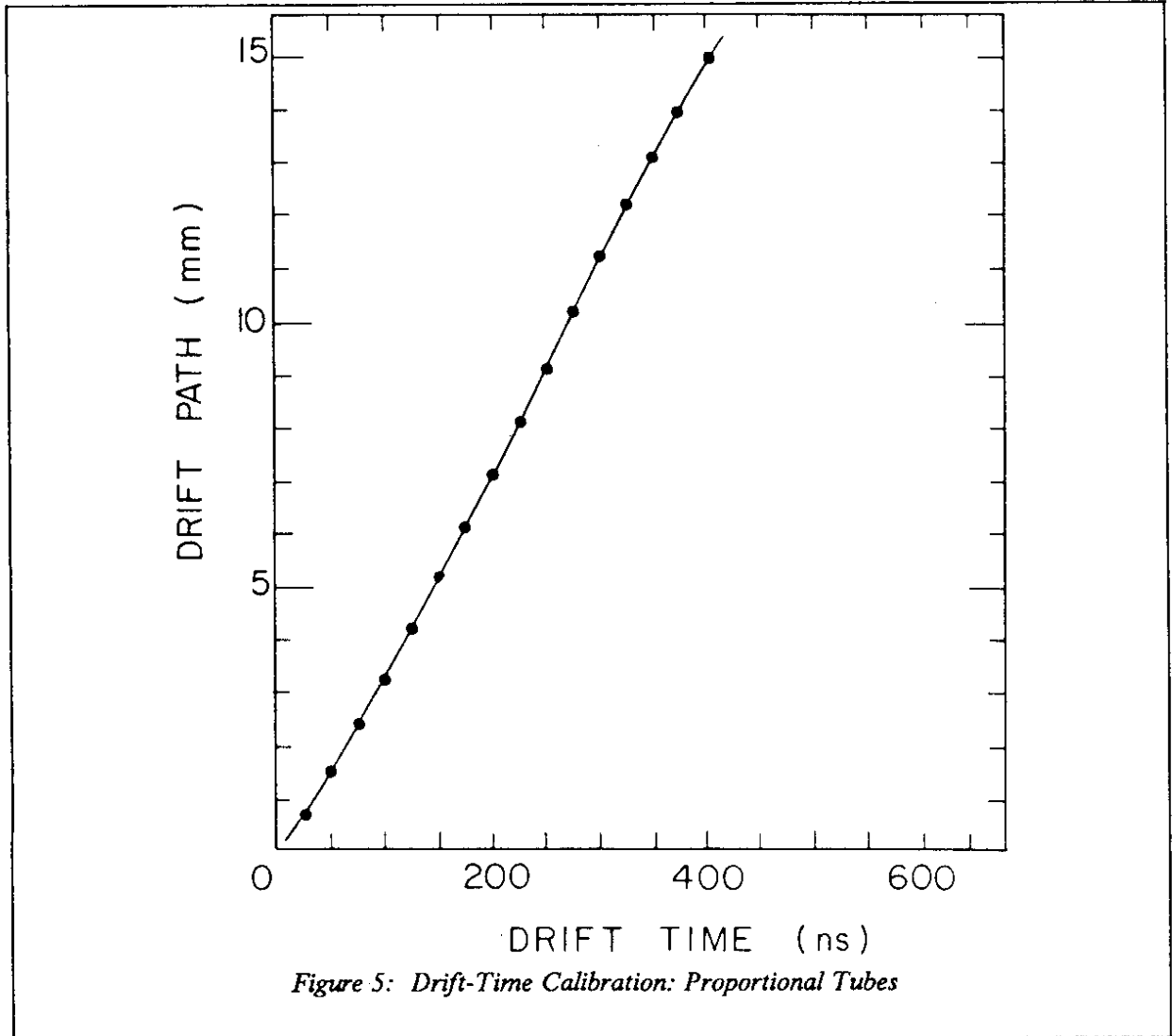
The response of this proportional tube system was also calibrated against the energy loss of cos-
mic-ray muons. The track-fitting procedure required at least four hits in each projection. With this re-
quirement, the muon tracks produced in charged-current neutrino interactions (or by cosmic-ray
muons) could be readily reconstructed by the analysis program. The identification of a muon in the fi-
nal state of a neutrino interaction was the element which enabled it to be classified as a charged-current
event. Conversely, the absence of such a muon was the signature of neutral-current neutrino interac-
tions, or the interaction of electron neutrinos. On the other hand, muon tracks fitted and found to
have entered the detector from the outside, could be often readily classified as cosmic-ray background
events and rejected accordingly.

The proportional tubes also provided information on the lateral vertex position of the neutrino interactions. The early part of a shower contains only a few charged tracks. The hit distribution of the proportional tube planes immediately downstream of the start of the shower, weighted by the pulse-height in each tube, was used to estimate the lateral coordinates of the vertex. An example of the measured lateral energy deposition by 10 GeV pions (averaged over many events) is shown in Figure 6.

Figure 6: Lateral Energy Deposition: Proportional Tubes

A further important role of the proportional tubes was in the determination of the shower direction [5]. Starting from a first estimate of the shower axis obtained by joining the shower vertex to its barycentre, which was derived from the energy deposition in the scintillators, an algorithm was used to refine the shower direction measurement based on the pulse-height recorded in the proportional tubes and their distance from the shower vertex and the current estimate of the shower axis. This iterative procedure found the straight line starting from the vertex which subdivided the energy deposition in each projection into two equal parts. Tube hits far from the shower axis were given less weight than those close to the the axis.

2.4 Streamer Tube System

The sampling of the CHARM calorimeter for energy deposition occurred after each marble plate (i.e. $\approx$ 1 rad. length). However, the sampling in spatial position by the proportional tubes occurred effectively only every two marble plates, since the measurements alternated between the horizontal and the vertical. This proved to be a limitation on the angular resolution with which the shower direction could be measured, particularly for electromagnetic showers. The emergence of the limited streamer tube [6] as an inexpensive detector of charged particles enabled this limitation of the CHARM Calorimeter to be overcome, by inserting a plane of such tubes, which were specially constructed for the purpose [3], [4], in between each marble plate.

The main aim of the streamer tubes was to improve the resolution of the measurement of the direction of electromagnetic showers produced in the scattering of muon-neutrinos by electrons:

$$\nu_\mu + e^- \rightarrow \nu_\mu + e^-$$

$$\text{and} \quad \bar{\nu}_\mu + e^- \rightarrow \bar{\nu}_\mu + e^-.$$

The results showing the improved resolution obtained are given in section 3.4.

The streamer tubes also gave improvements in the vertex resolution and in the energy flow measurements of hadronic showers, as well as giving an independent energy sampling of the showers based on the number of fired tubes.

Because the streamer tubes provide only a "hit" distribution, saturation in the energy response occurs for high-energy hadron showers, due to the fact that more than one particle can hit the same tube. Electromagnetic showers are even more dense and saturation occurs at quite low energy. This effect was used to help separate electromagnetic and hadronic showers by comparing the number of "holes" (i.e. non-fired tubes) in the shower region with the number expected for an average electromagnetic shower of the same energy.

Improved measurements of both the vertex and the shower angle were obtained by using the streamer tubes in a way analogous to the use of the proportional tubes described before. Thus in the first gap after the shower vertex, one projection was well measured by the proportional tubes and the other by the streamer tubes. For the measurement of the shower angle, both proportional and streamer tubes were used independently as well as in combination weighted by the inverse of their respective resolutions.

3. Calibration Measurements

3.1 Beam and Test Installation

For the purposes of calibration, 36 of the 78 subunits of the target calorimeter were installed in a charged particle beam at CERN whose energy could be varied from 5 to 140 GeV. In order to study the response of this structure to very low energy particles, a smaller copy of the calorimeter was constructed by the Moscow members of the Collaboration, and exposed to a beam of energies 0.5 - 6 GeV at the Institute for Theoretical and Experimental Physics, Moscow. The details of this low energy calibration will be published [7] elsewhere, but for completeness, the results will also be presented here.

Figure 7 shows the beam lay-out and the arrangement in the experimental hall 182 at CERN. The charged particle beam was brought alongside the neutrino beam line in the experimental hall so that the installation of the 36 calorimeter subunits could be achieved by a simple translation of their position. Two 5 m long bending magnets allowed the beam to be deflected horizontally in order to study different impact points and angles at the detector. Beam profile counters were used to determine
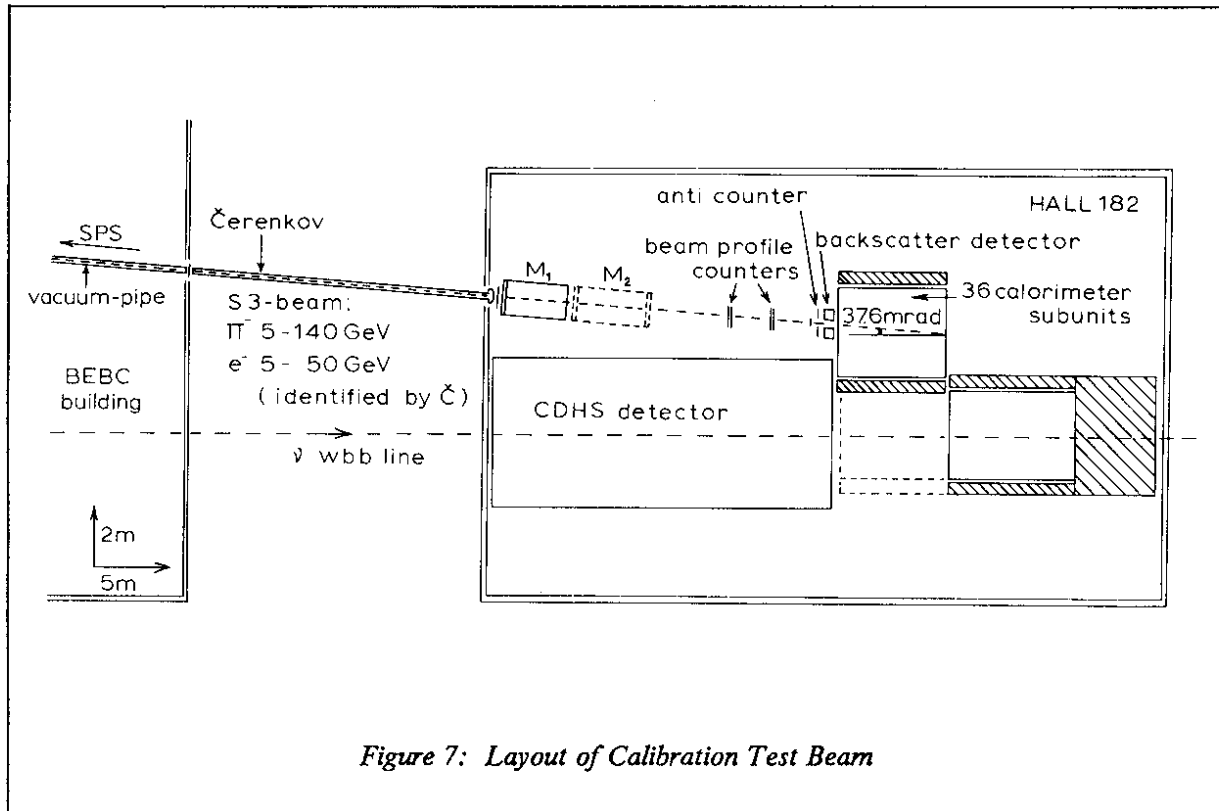
Figure 7: Layout of Calibration Test Beam

the impact point on the first calorimeter plane. An anti-counter allowed the rejection of particles outside the defined beam acceptance. In the undeflected beam position, a backscatter detector could be placed in front of the calorimeter. This was used to determine the energy deposition of backward scattered particles as well as to investigate the development of electron showers with a vertex at different depths of marble in the calorimeter.

The test beam of negative pions and electrons, produced by the interaction of 200 GeV protons from the SPS, had a momentum range of 5 to 140 GeV/c for pions and of 5 to 50 GeV/c for electrons. The central beam momentum was known to $\pm 1\%$, the fractional momentum spread was about 0.75%. For measurements with the pion beam, a beryllium target (150 mm long) was used; for the electron beam an aluminium target of 100 mm length was chosen to increase the yield of electrons compared to pions. Above 50 GeV/c the electron component of the beam was less than 1%. When a pure pion beam was needed, a lead filter was placed in the beam just upstream of one of the bending magnets. The beam intensity was adjusted to around 10 to 20 particles per burst in a 30 ms spill.

This test beam was transported in a vacuum pipe up to the Cherenkov counter. The 20 m long helium-filled threshold Cherenkov counter permitted the tagging of electrons up to 30 GeV/c. 50 GeV/c electrons were identified by the width of their shower profile. The beam profile counters were multi-wire chambers of 1 mm wire spacing with a sensitive area of 64×64 mm^2. Each set had 2 orthogonal planes of wires; the two sets were spaced by about 1 m. The anti-counter was a lead/scintillator sandwich with two lead plates of 2 cm thickness each, interleaved by a 6 mm thick scintillator. The sensitive area was about 1 m^2, with a central hole of 45×45 mm^2 diameter, for the passage of the beam particles.

The backscatter detector, shown in Figure 8, had a structure identical to the target calorimeter. It consisted of 2 marble planes of the same thickness (8 cm) as those in the target calorimeter, each one

Figure 8: Detail of the Backscatter Detector
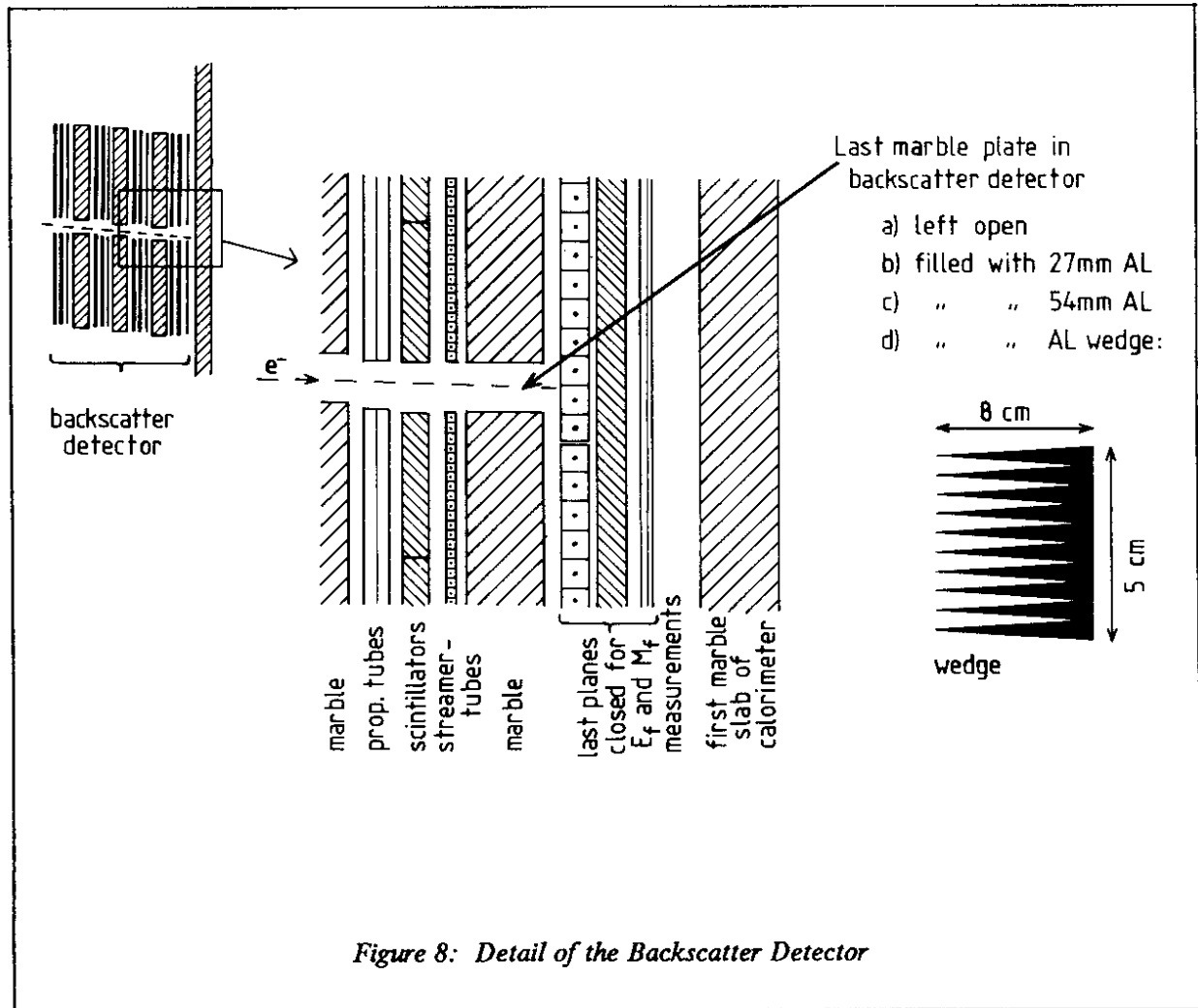
being made of two halves. The 2 marble planes were imbedded in 3 planes of detection elements, each composed of proportional drift tubes, scintillators and streamer tubes in the same alternating orientation as in the calorimeter. The arrangement of marble plates and detection elements was such that it left a free passage for the beam particles of about 50×50 mm^2; the outside dimensions of this apparatus were 1×1 m^2. The most downstream detection planes of the backscatter detector with proportional drift tubes, scintillators and streamer tubes, could be moved such that they also covered the free beam passage behind the last marble plane. This arrangement was used to investigate the development of electron showers with marble plates of different thickness placed in the slit of the last marble plane.

The backscatter detector was used only for measurements in the undeflected beam position T; for the other measurements it was taken out without changing the disposition of either the anti-counter or the beam profile counters. Table 1 gives details of the impact points chosen and of the beam direction in the horizontal and vertical planes of these points. During beam steering, a scintillation counter was inserted before and a scintillator hodoscope after the Cherenkov counter; for all real measurements they were moved out of the beam.

Table 1: Beam Parameters for Calibration Measurements

code name	impact-points (in mm)		impact-angles (in mrad)	
	Horiz.	Vert.	Horiz.	Vert.
R	− 240	71	− 67.6	− 8.65
T	+ 273		− 37.6	
A	+ 1020		+ 6.1	
L	+ 1150	71	+ 13.7	− 8.65

A beam of incident particles was defined by the absence of a signal from the anti-counter, and a coincidence of the signals from two beam scintillation counters. The first, of dimensions 100×100 mm^2, was located at the entrance of the bending magnets. The second, of dimensions 50×50 mm^2, was located in front of the anti-counter. For electron measurements, signals from the Cherenkov counter in coincidence with the incident particles were used, with the gas pressure set below the threshold for pions. The calorimeter was read out if at least four scintillator planes were hit. Events induced by pions were required to have not more than one hit in the first two scintillator planes and in the first plane of proportional drift tubes to avoid beam halo. In the analysis, events were selected if each hodoscope of beam profile counters and the scintillators had registered only one incoming particle and if no signal was present from the veto counter in time with the beam particle.

3.2 Use of the Backscatter Detector

Relativistic kinematics restricts backscattering to the products of nuclear break-up which have an almost isotropic angular distribution. The purpose of the backscatter detector was to enable studies to be made of the frequency of occurrence of this phenomenon and its effect on the determination of the shower vertex position by the various routines in the analysis program.

For such tests, pion-runs with an open backscatter detector were chosen, and only events starting in the first plane were used in the analysis. A criterion was needed to determine that the shower indeed started in the first plane. At least two streamer-tube and at least two proportional-tube hits were required. This criterion was not perfect; a passing pion could, for example, fulfil this criterion and then interact ten planes later. A stronger criterion would have caused a bias in shower selection, hence it was accepted that a small contamination of events starting actually in a later plane was present in the data sample. However, it is certain from the detector set-up that no event started before the first plane and thus the influence of backscattering could be investigated.

The percentage of pions interacting in the first plane selected according to this criterion was compatible with the percentage predicted from the known properties of marble and the pion interaction cross-section.

The percentage of events with any backscatter hit, a backscatter hit in a scintillator, a proportional-tube or a streamer-tube is shown in Figure 9. versus the energy of the incoming pion. The scintillator system is evidently more strongly affected by backscattering than the tube systems. This occurs since backscattering is produced mainly by low-energy nucleons from nuclear breakup, and gaseous detectors are sensitive only to charged particles whereas scintillators also detect neutrons.
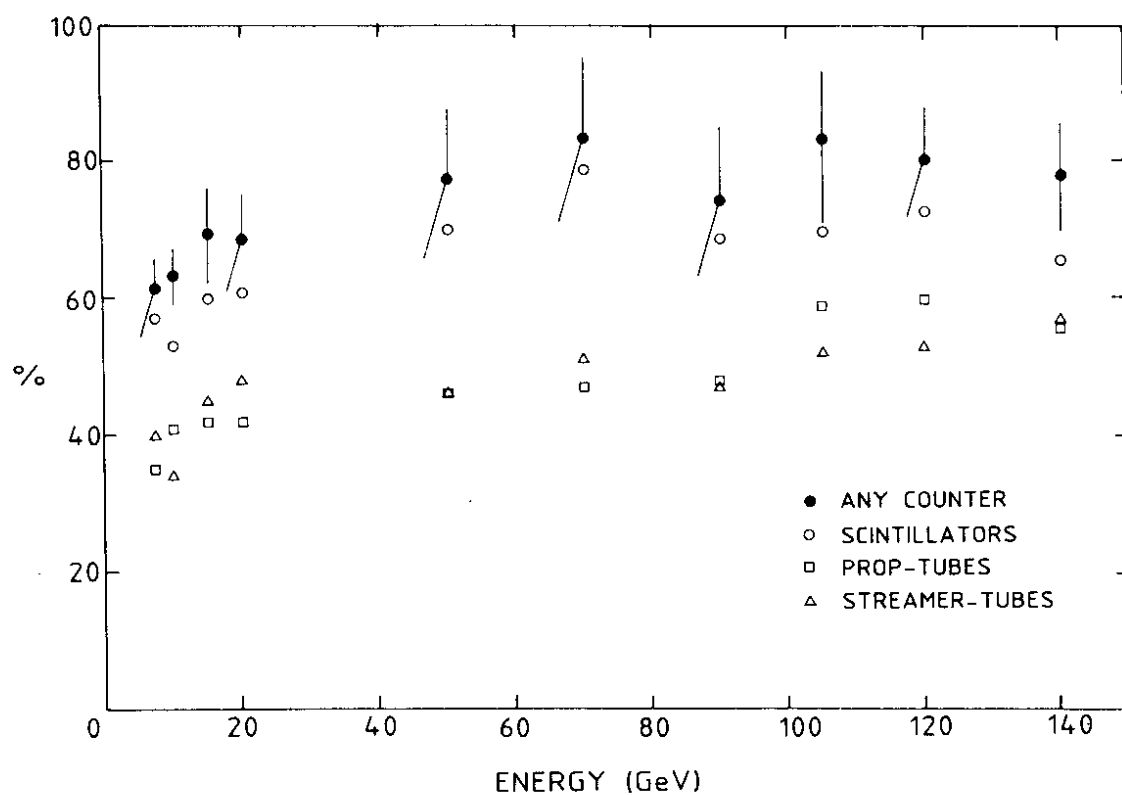
Figure 9: Percentage of Events with Backscattering

Table 2:   *Mean Backscattered Energy for Different Beam Energies*

Beam Energy [GeV]	E(Backscatter) [GeV]
7.5	0.15
10.0	0.16
15.0	0.16
20.0	0.17
50.0	0.19
70.0	0.18
90.0	0.18
105.0	0.16
120.0	0.17
140.0	0.20

Despite the high frequency at which backscattering occurs, the average energy contained in the backscatter is small and rather independent of the beam energy, as shown in Table 2. However the backscatter energy distribution has a long tail to high energies, so individual events can have deposition of several GeV.

The data taken were used to study algorithms to correct the error in the determination of the start-plane of the true shower. These were based on the principle that backscattering produces energy deposition which in addition to being upstream of the true shower vertex, is frequently far away from the axis of the shower. Thus if the comparison between the position of the barycentre of the scintillators in the first plane of a shower was inconsistent with the position expected by extrapolating back the shower axis (determined from the subsequent three planes in each projection), the start-plane of the shower was taken to be one plane further downstream, and the energy deposition in the first active plane was assumed to be due to backscattering. The same data were also used to study and improve the various algorithms to determine the lateral shower vertex.

3.3 Energy Calibration Measurements

The calibration of the energy response of the calorimeter to hadrons and electrons was performed using the apparatus described in section 3.1. For the calibration with hadrons, beams of π^- with energies from 5 to 140 GeV were used. For electrons, the range was 5 to 50 GeV.

The principal tool used for the energy measurement was the response of the scintillation counters to the charged particles in the cascade. However, both the proportional drift tubes and the streamer tubes were used for energy measurements, albeit with poorer resolution. Calibration of the proportional tubes was necessary since they were the only detectors present in the iron frame around the marble and in the end calorimeter. Calibration of the streamer tubes enabled an independent measure of the energy deposit to be made and was based on the number of "hits" in the streamer tubes produced by a known shower.

Data were taken at each given beam energy and the total shower energy was obtained by summing the outputs of the scintillators (and the proportional tubes) covering the region of the shower. For this the raw electronic signals from each scintillator were first corrected for light attenuation and the signals from both scintillators and proportional tubes were converted into energies (referred to as E_{vis}) via the comparison with the known response of the same detectors to cosmic-ray muons as described in section 2.2. Thus E_{vis} is the number of normally incident cosmic-ray muons traversing a single detector plane which would produce the same electronic response multiplied by the known energy deposition by one normally incident muon at the mean energy of the muons accepted by the cosmic-ray trigger (7.4 MeV for scintillators). An example of the response of the scintillators to π^- is shown in Figure 10. At higher energies, the response curves show a tail towards lower E_{vis} because of leakage. The procedure used to extrapolate the response for an infinitely long calorimeter has been described previously [2].

The response of the detector was defined as the fraction of the energy E which was observed in the scintillators (or proportional tubes).

$$F = E_{vis}/E$$

The energy resolution was defined as the r.m.s. deviation of the visible energy from its mean value (derived from a Gaussian fit) divided by the mean value.

$$R = \sigma(E_{vis})/<E_{vis}>$$

Since the test installation contained only 36 planes of the detector, at higher energies hadronic showers were not completely contained. The longitudinal energy deposition shows some leakage at the
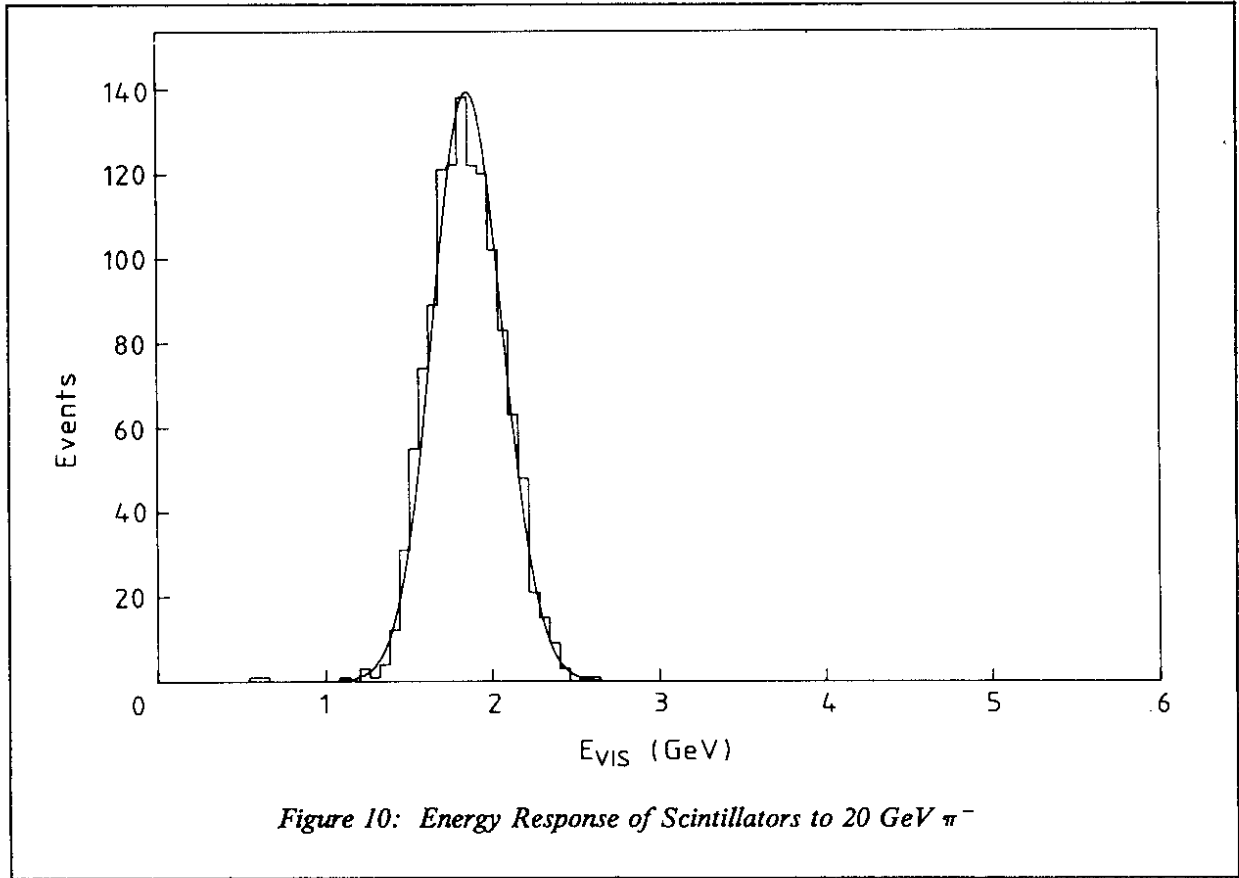
Figure 10: Energy Response of Scintillators to 20 GeV π^-

downstream end, particularly for showers which start late in the calorimeter. At each beam energy, the mean longitudinal scintillator shower profile was evaluated by superposition of all showers where the plane showing the highest energy deposition was used to adjust the longitudinal position of each shower to correct for the differing start planes. If a shower started after the 16th plane, or had its maximum-energy plane after the 30th plane, it was not used for this analysis.

From this shower profile, it was possible to deduce the fractional hadronic energy leakage, α, as a function of the beam energy, and this could then be used to correct for the leakage at high energies. The fractional leakage beyond N planes (measured from the vertex plane) could be parametrized as:

$$\alpha = 2.55 \exp(-0.440 N/E^{0.2})$$

where E was the beam energy in GeV. The effect of this correction was a maximum of 0.7% at 140 GeV.

A further correction was applied to take account of the energy deposition of the incoming pion before the start of the shower. Unlike neutrino induced showers, the energy seen in front of the shower region was added to that found inside the shower region in order to record the full energy deposition of the incident particle.

After applying these corrections, the mean value of the energy response and the r.m.s. deviation of the distributions at each energy, normalised to this mean, were computed from a Gaussian fit. The results are shown in Table 3, for both scintillators and proportional tubes.

Table 3: Hadronic Energy Response and Resolution

Beam Energy (GeV)	Scintillators response $F_S(\times 10^2)$	Scintillators resolution R_S (%)	Proportional Tubes response $F_p(\times 10^5)$	Proportional Tubes resolution R_p (%)
7.5	8.88 ± 0.03	19.49 ± 0.3	8.87 ± 0.05	28.60 ± 0.4
10.0	8.99 ± 0.03	16.87 ± 0.2	9.15 ± 0.04	24.45 ± 0.3
15.0	9.20 ± 0.01	13.71 ± 0.1	9.29 ± 0.02	21.04 ± 0.2
20.0	9.20 ± 0.01	12.43 ± 0.1	9.01 ± 0.02	18.34 ± 0.2
30.0	9.50 ± 0.02	10.91 ± 0.1	9.18 ± 0.03	16.82 ± 0.2
50.0	9.48 ± 0.01	8.25 ± 0.1	8.80 ± 0.02	14.22 ± 0.1
70.0	9.59 ± 0.01	7.17 ± 0.1	8.63 ± 0.02	13.50 ± 0.2
120.0	9.64 ± 0.01	5.56 ± 0.1	8.43 ± 0.02	11.70 ± 0.2
140.0	9.59 ± 0.01	5.24 ± 0.1	7.96 ± 0.03	13.29 ± 0.2

These results were fitted to give a parametrization of the energy dependence of the response and resolution of the scintillators and proportional tubes to incident hadrons, yielding:

Scintillators:

hadron response	$F_S(\text{hadr.}) = [(9.62 - 257/(E^2 + 315)) \pm 0.05] \times 10^{-2}$
hadron resolution	$R_S(\text{hadr.}) = [(48.7/\sqrt{E} + 1.27) \pm 0.3]\%$

Proportional Tubes:

|	
hadron response	$F_p(\text{hadr.}) = [(10.4 - 0.19\sqrt{E}) \pm 0.4] \times 10^{-5}$
hadron resolution	$R_p(\text{hadr.}) = [(44.3/\sqrt{E} + 8.1) \pm 1.8]\%$

where the energy E is in GeV. Hence the hadronic shower energy could be computed from the scintillator energy (E_{vis}) from the formula:

$$E = E_{vis}[10.40 + 1.85/(E_{vis}^2 + 1.5) - 0.0376/(E_{vis}^2 + 0.014)].$$

The corresponding response function ($F_S(\text{hadr.}) = E_{vis}/E$) is shown in Figure 11, together with the data from these measurements (open points) and the data taken at the Institute of Theoretical and Experimental Physics, Moscow (solid points) using a smaller copy of the calorimeter in a beam of energies 0.5 - 6 GeV [7]. For these latter data, which were normalized to the CERN data using the electron response at 5 GeV, the energy E was the kinetic energy of the beam, since hadron masses cannot be neglected at low energies.

An equivalent procedure to that described above was carried out for the calibration of the response of the scintillators and proportional tubes to electrons. In this case, no leakage correction was necessary, even at the higher energies, since electromagnetic showers were well contained in the 36 planes of the calorimeter used for calibration. An example of the energy response of the scintillators to e^- is shown in Figure 12.

The response and resolutions of the scintillators and proportional tubes to electron beams were evaluated as before, and the results are given in Table 4. These results were fitted to give a parametrization of the energy dependence of the response and resolution of the scintillators and proportional tubes to incident electrons, yielding:

Figure 11: Scintillator Hadron Response Function F_S(hadr) vs. $\sqrt{E}$
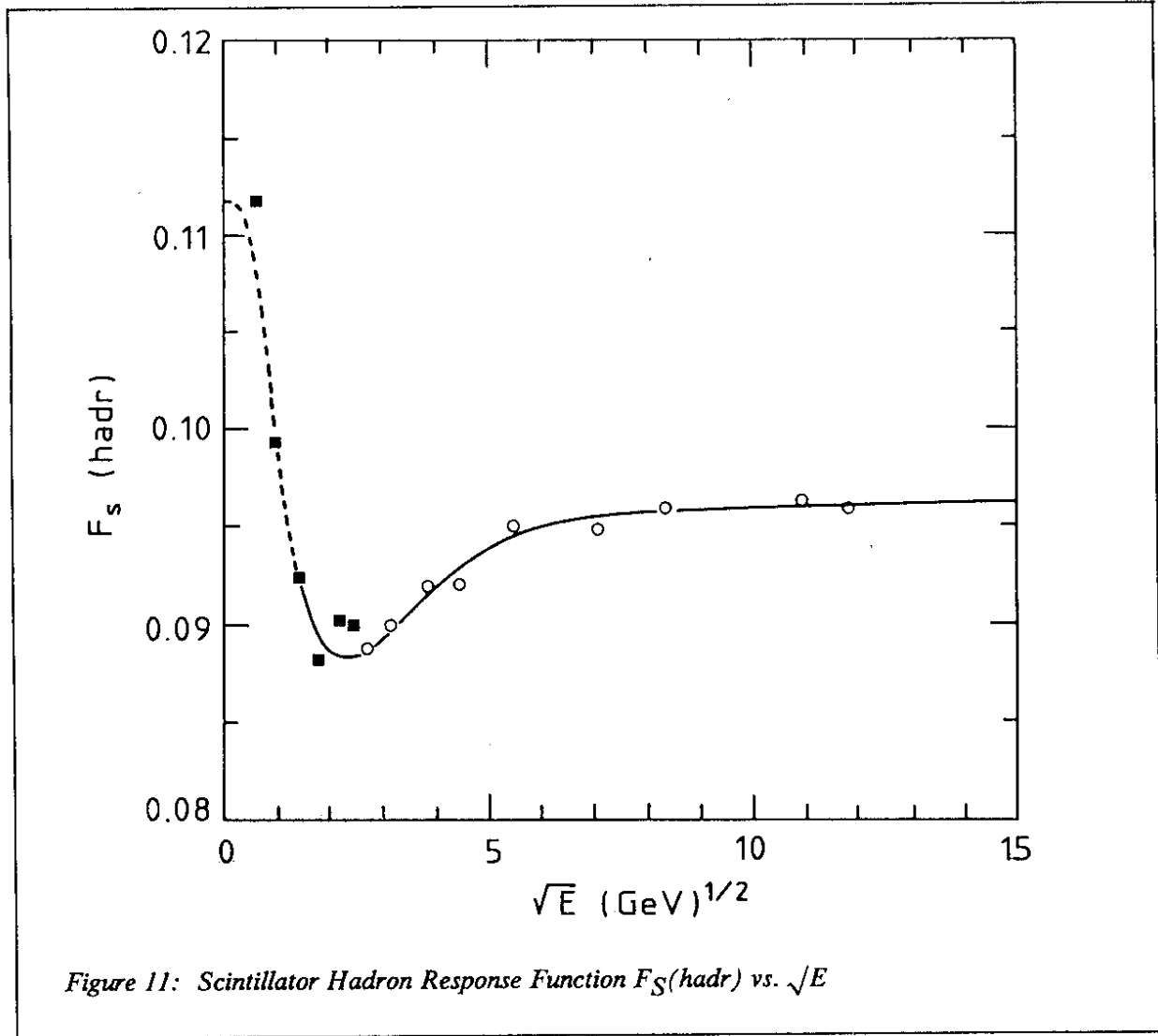
Scintillators:

electron response F_S(elec.) $= [11.3 \pm 0.3] \times 10^{-2}$

electron resolution R_S(elec.) $= [(18 \pm 1)/\sqrt{E}]\%$

Proportional Tubes:

electron response F_P(elec.) $= [(13 - 0.7\sqrt{E}) \pm 0.5] \times 10^{-5}$

electron resolution R_P(elec.) $= [(17.5 - \sqrt{E}) \pm 2]\%$

where the energy E is in GeV.

Hence for electromagnetic showers, the shower energy could be evaluated simply from the visible energy in the scintillators as $E = E_{vis}/11.3$. The resolution obtained with the scintillation counters for both hadronic and electromagnetic showers is shown in Figure 13 where $R_S\sqrt{E}$ is plotted as a function of $\sqrt{E}$.

The calibration of the streamer tubes involved recording the mean number of tube "hits" at each beam energy. As already mentioned in section 2.4, the response of the streamer tubes saturates at quite
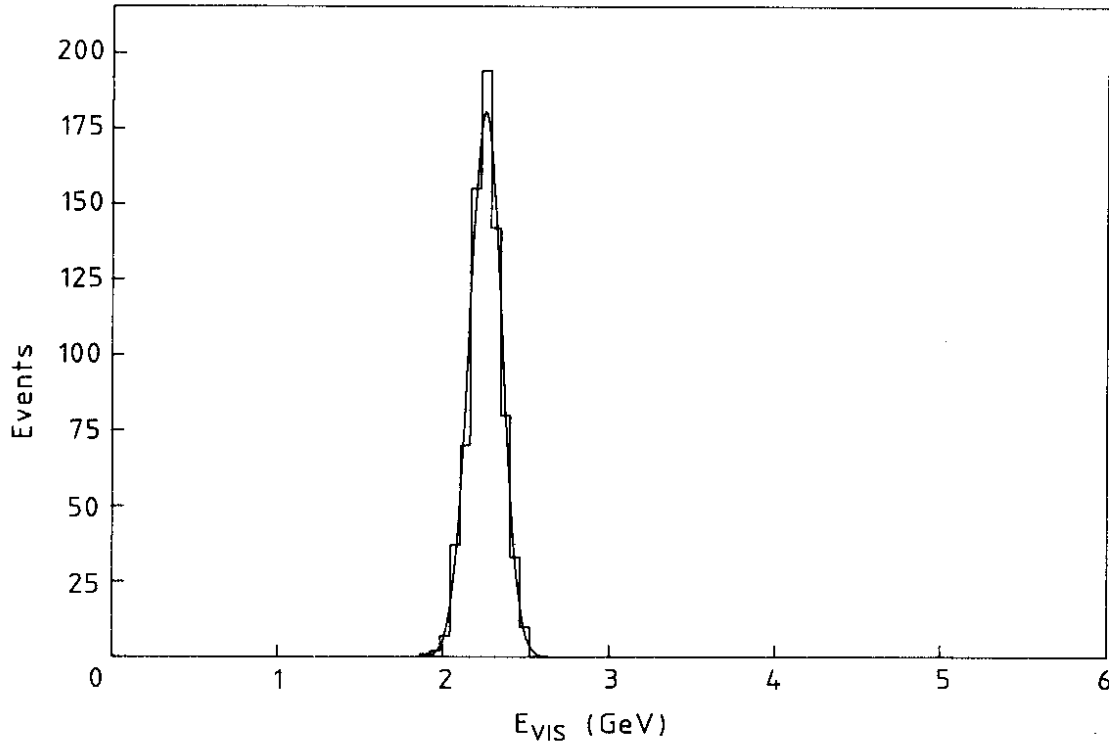
Figure 12: Energy Response of Scintillators to 20 GeV e⁻

*Table 4: Electromagnetic Energy Response and Resolution*

Beam Energy (GeV)	Scintillators		Proportional Tubes	
	response $F_S(\times 10^2)$	resolution R_S (%)	response $F_P(\times 10^5)$	resolution R_P (%)
5.0	11.3 ± 0.3	8.0 ± 0.4	11.5 ± 0.3	15. ± 2.
7.5	11.3 ± 0.3	6.7 ± 0.3	10.5 ± 0.5	15. ± 2.
10.0	11.3 ± 0.3	5.8 ± 0.3	10.5 ± 0.5	14. ± 2.
15.0	11.2 ± 0.3	4.8 ± 0.2	10.2 ± 0.5	12. ± 2.
20.0	11.2 ± 0.3	4.2 ± 0.2	9.3 ± 0.5	16. ± 2.
30.0	11.4 ± 0.3	3.3 ± 0.4	8.3 ± 0.5	15. ± 2.
50.0	11.1 ± 0.5	2.4 ± 0.4	8.1 ± 0.5	11. ± 3.

modest energies, particularly for electromagnetic showers. This effect is clearly seen in Figure 14, where the number of "hits" is plotted against the beam energy for both π^- and e^- beams.

Figure 13: Energy Resolution of Scintillators vs. $\sqrt{E}$
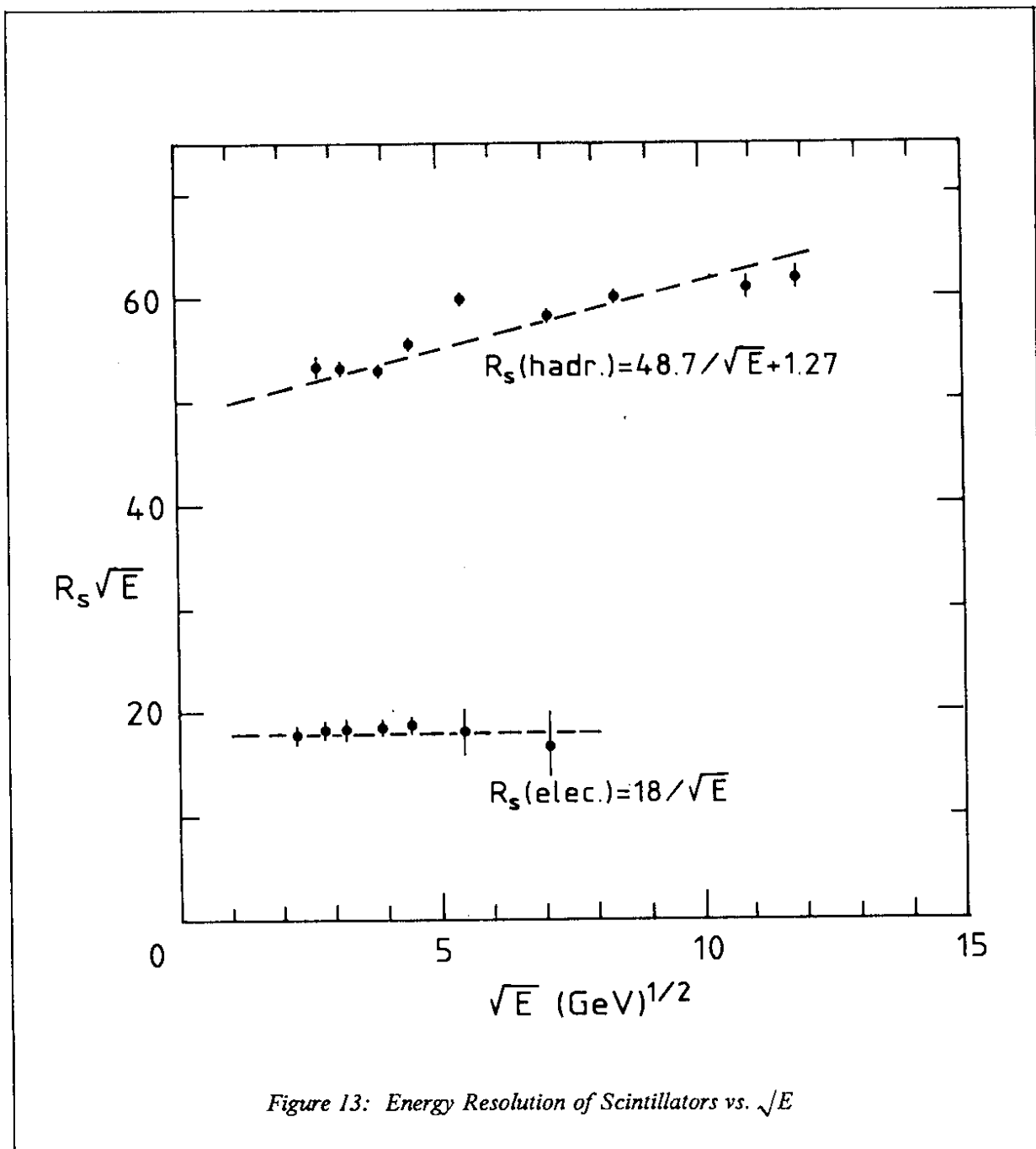
3.4 Shower Direction Measurements

The test set-up (described in section 3.1) contained beam profile counters which allowed the trajectory of the incoming particles to be defined. Hence the vertex of the interaction could be determined by extrapolation of this trajectory to the start-plane of the shower. The resolution of the calorimeter in determining the lateral shower vertex could then be measured by comparing this beam vertex with that determined purely from the analysis of the shower data.

Figure 14: Response of the Streamer Tubes to π^- and e^-
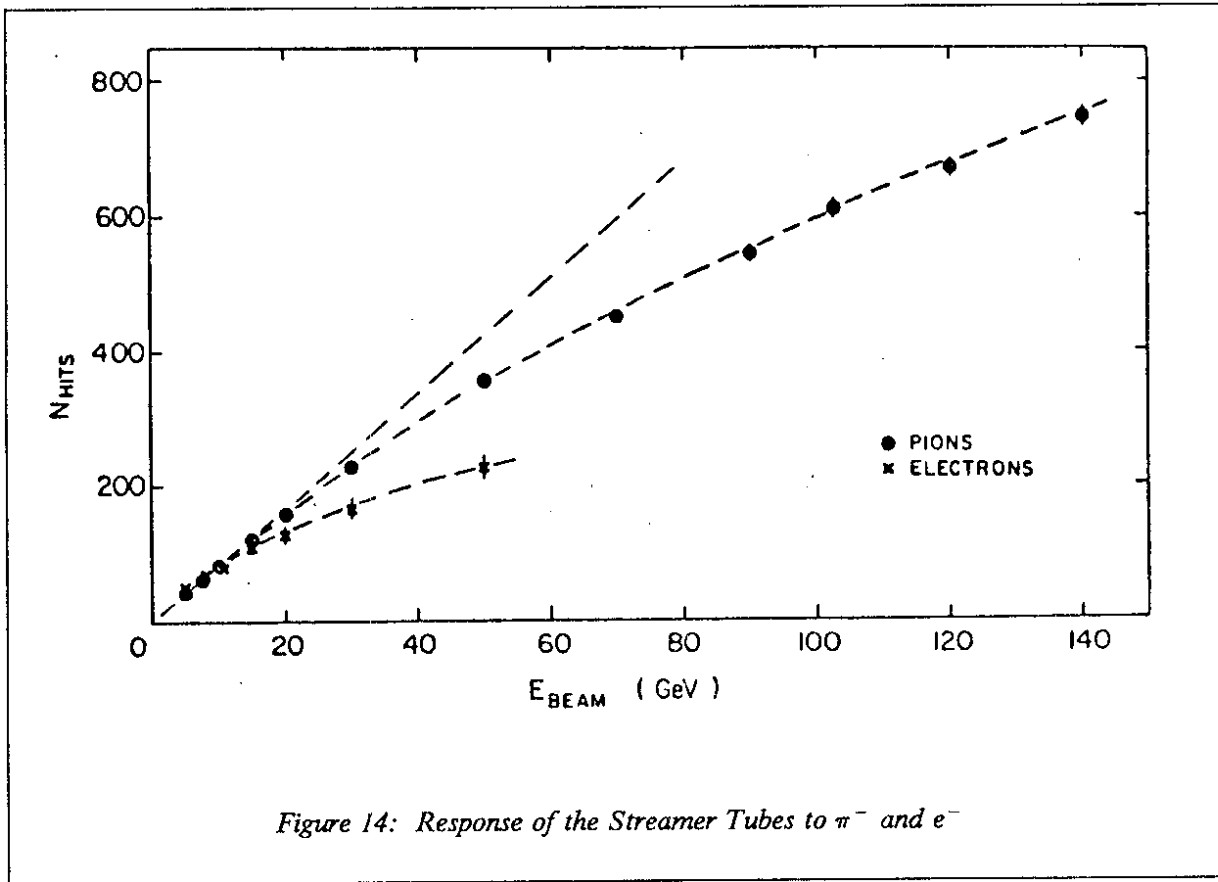
Since the streamer tubes were added to improve the resolution on the lateral vertex position (as well as the shower angle resolution), Figure 15 displays the energy dependence of the r.m.s. resolution on this vertex determination from the proportional tubes alone (broken line) and when both proportional and streamer tubes are used (solid line).

The vertex resolution obtained using pions was parametrized as follows:

Without Streamer Tubes: $\sigma_H(x) = 16.2/\sqrt{E} + 0.014E$ (cm)

With Streamer Tubes: $\sigma_H(x) = 14.9/\sqrt{E} + 0.006E$ (cm)

Similarly, the direction of the showers as measured by the shower properties alone could be compared with the known beam direction. Again the comparison is made of two situations in Figure 16, where the broken line indicates the energy dependence of the r.m.s. resolution on the projected shower angle from the π^- beam data without the use of the streamer tubes, and the solid line shows the improvement with their addition where the average of the two projections is shown. The curves of Figure 16 can be parametrized as follows:

Without Streamer Tubes: $\sigma_H(\vartheta) = 238/\sqrt{E} + 241/E$ (mrad)

With Streamer Tubes: $\sigma_H(\vartheta) = 141/\sqrt{E} + 520/E$ (mrad)

Figure 15: Hadronic Vertex Resolution with and without Streamer Tubes
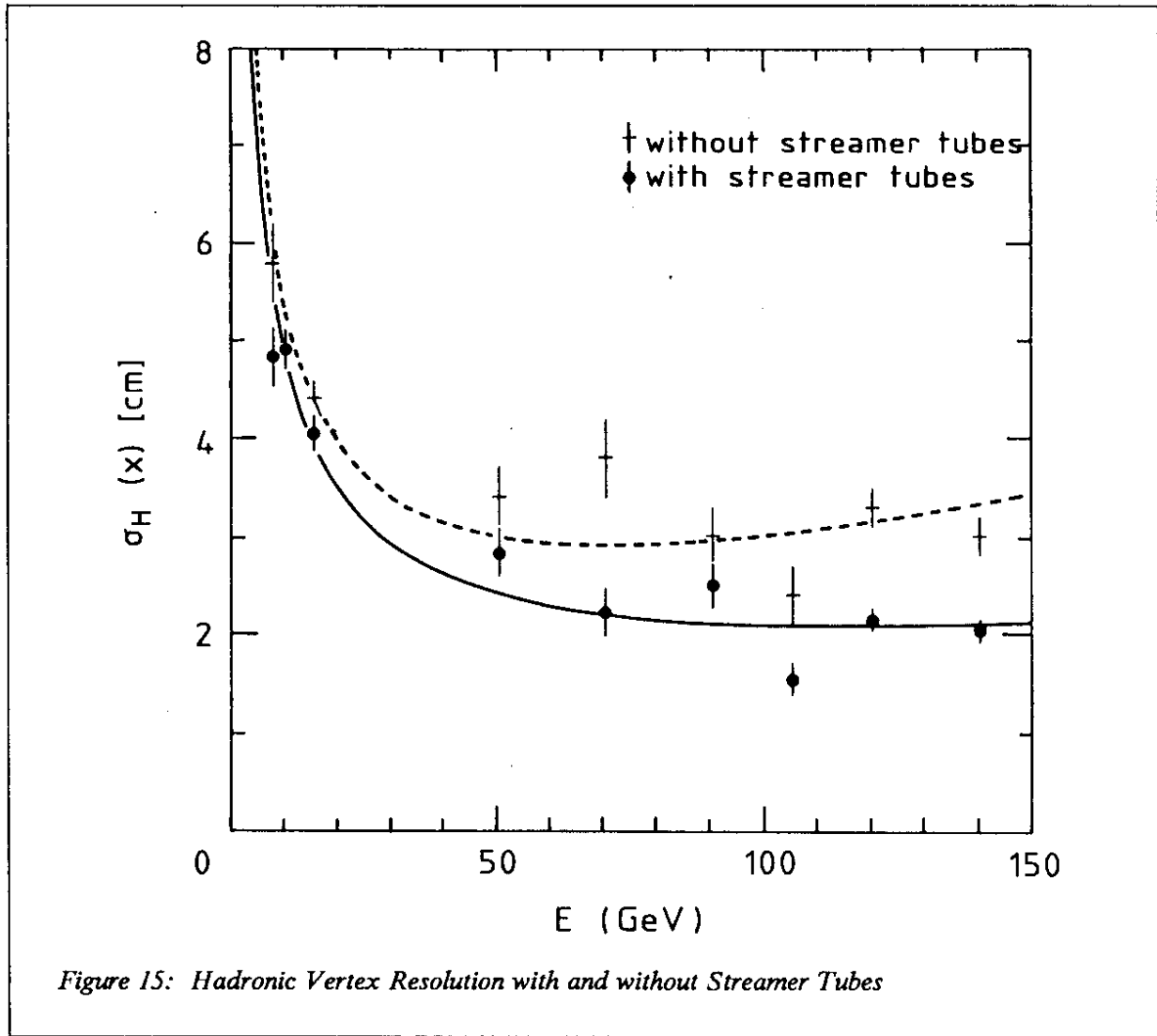
The equivalent situation for electromagnetic showers is shown in Figure 17, where the open points show the energy dependence of the r.m.s. resolution on the projected shower angle from the e^- beam data without the use of the streamer tubes, and the solid points show the improvement with their addition.

The parametrizations of the curves of Figure 17 are:

Without Streamer Tubes: $\sigma_e(\vartheta) = 46/\sqrt{E}$ (mrad)

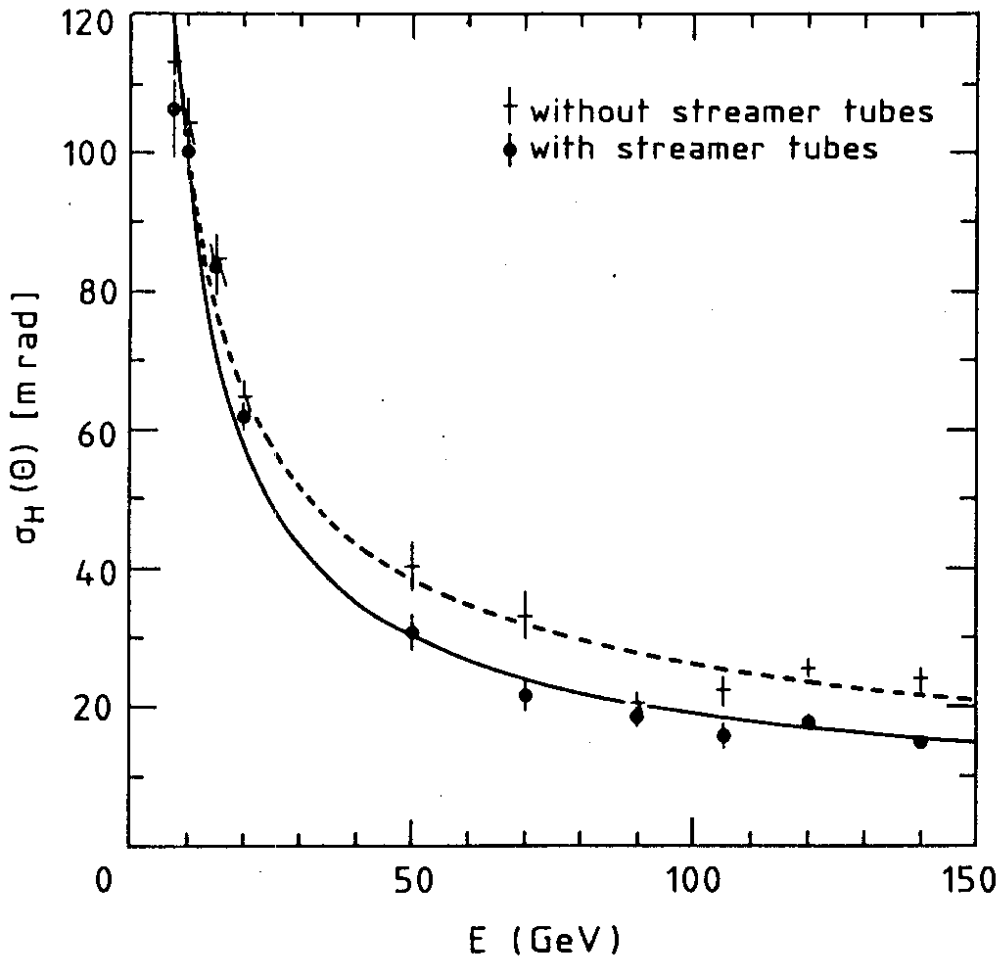With Streamer Tubes: $\sigma_e(\vartheta) = 32/\sqrt{E}$ (mrad)

Figure 16: Hadronic Shower Angular Resolution with and without Streamer Tubes

3.5 Electron-Pion Separation

The calibration test beam was used intensively to understand the different response to electromagnetic showers, represented by electron beam data, and to hadronic showers, represented by π^- beam data. As a result it was possible to define a "signature" by which electron showers could be recognized whilst allowing pion showers to be rejected.
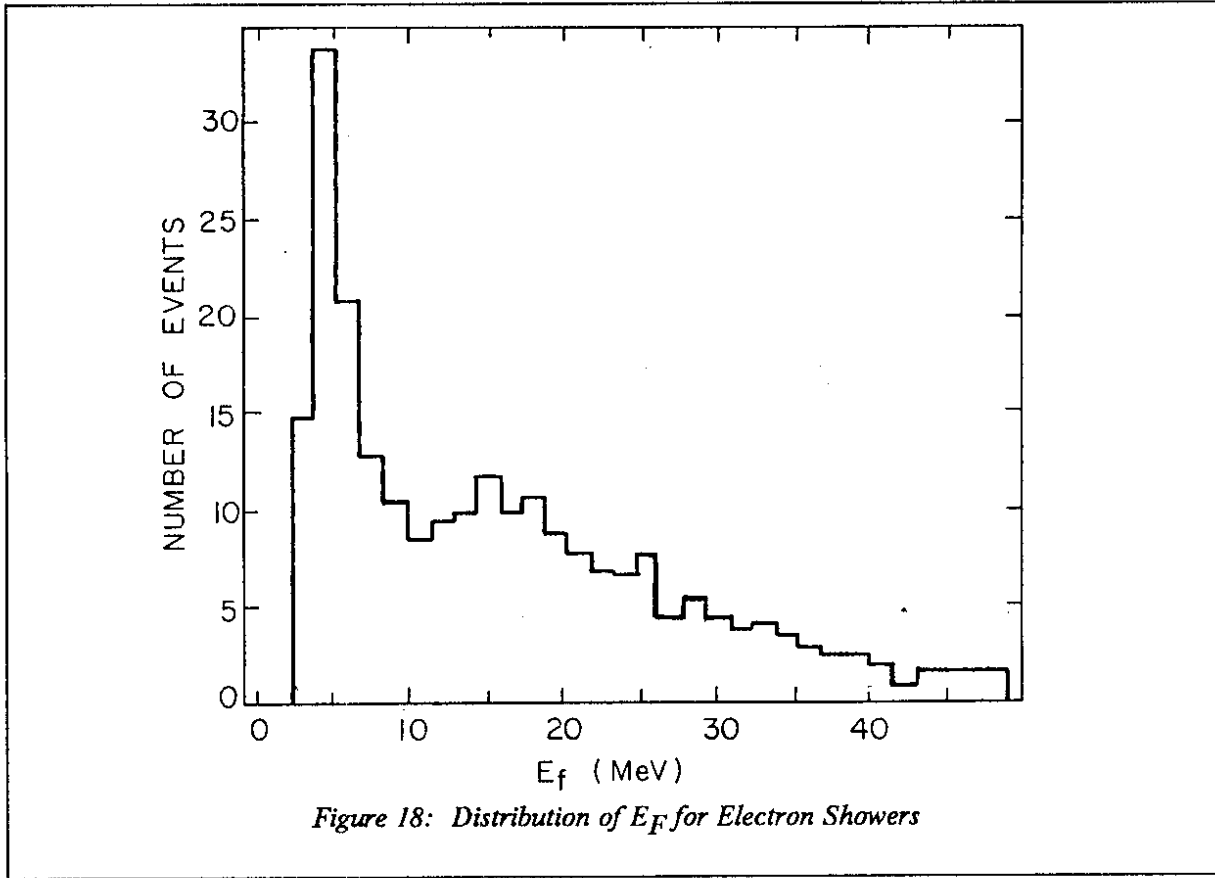
The electron signature in the CHARM calorimeter is based on the following general characteristics of electron showers. Close to the vertex (0.5 - 1 radiation length) the number of charged shower particles is in general odd, being 1 (in about 30% of the cases) or 3 (in about 10% of cases) or more; the probability of observing 2 particles is very small. A distribution from 15 GeV electrons measured after 0.5 radiation lengths shown in figure 18 demonstrates this property.

The lateral distribution of the energy deposited by the shower in a detector plane is regularly distributed in a disk centred around the direction of the primary electron with a radius R_M, where R_M is the Moliere radius given by $21 \text{MeV}/E_{crit}$. For low Z material where the critical energy is high, R_M is smaller than one radiation length. The appearance of energy tails generated by energetic particles off-axis is quite exceptional for electromagnetic showers in contrast with hadronic showers.

*Figure 17: Angular Resolution for Electromagnetic Showers*
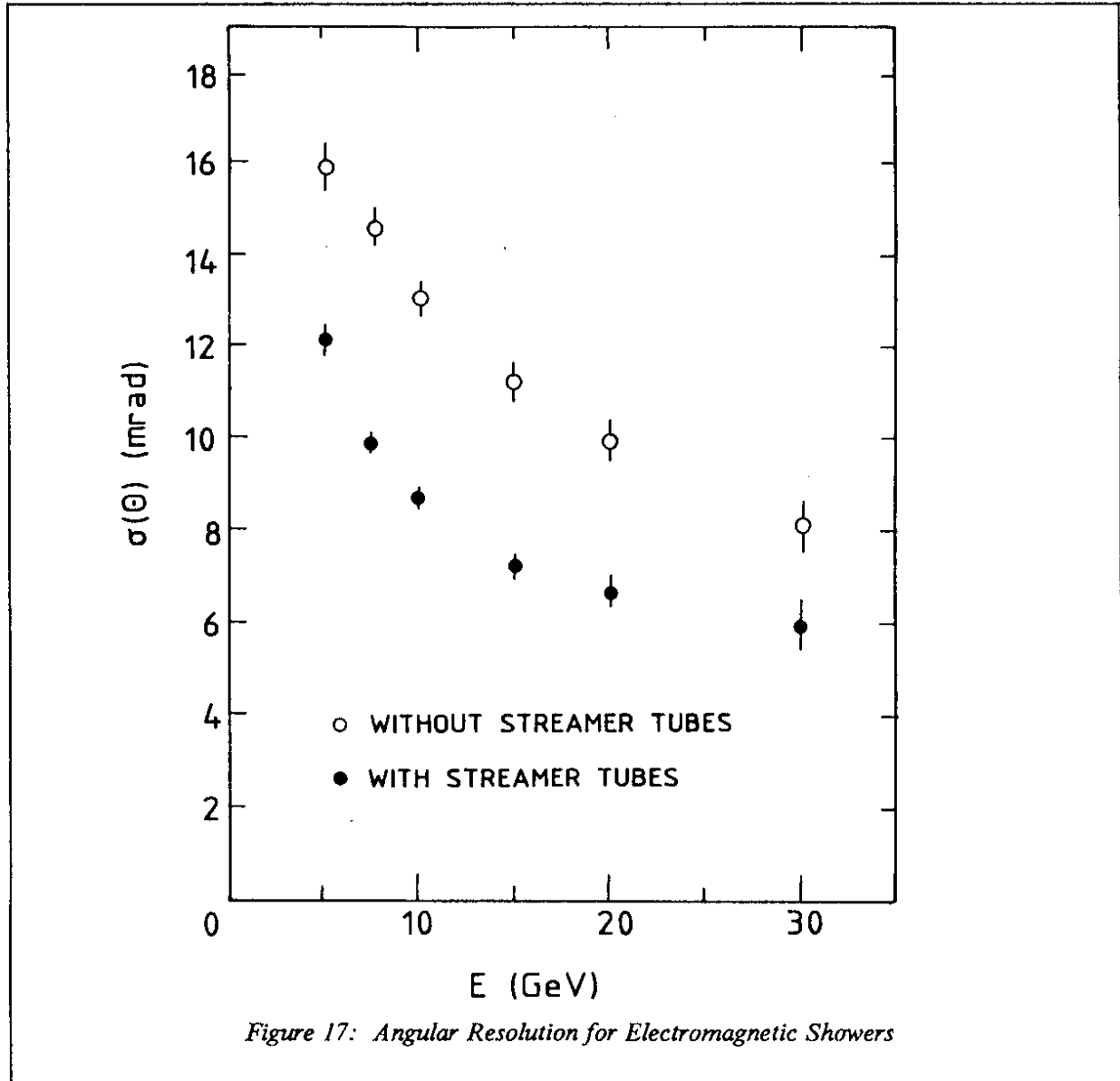
The characteristics mentioned above are reflected in the space distribution of the signals from the three detector components of the calorimeter. These include a plastic scintillator plane, a plane of proportional counters and a digital (yes, no) streamer-tube plane for every one radiation length of marble, which extends over 20cm longitudinally. The shower characteristics can be transformed into mathematical estimators for electron-hadron separation in a very simple way.

1. The energy deposited in the first plane E_F is defined by the signal on the scintillator. Showers initiated by a single electron can be defined by the condition $E_F \leq 2E_{MIP}$ (≈ 12.5 MeV), where E_{MIP} is the energy deposited by one minimum ionising particle (an energetic muon). A selection $E_F \leq 8$ MeV can be used to identify single electrons in the presence of showers initiated by more than one electron, for example those produced by photons or π^0 decays.

*Figure 18: Distribution of E_F for Electron Showers*

2. The projected lateral energy distribution in the scintillators (which have transverse dimensions of 15cm) can be described by a Cauchy distribution of width Γ. Electron showers have $\Gamma \leq$ 1cm (for 90% containment) in the CHARM calorimeter as shown by the calibration data where well identified electrons are incident on the Calorimeter (Fig. 19).

3. The lateral tails of the showers are well measured by the proportional planes which extend over the full detector area and allow for the largest fiducial volume. The root mean square (σ) of the energy distribution is used to measure the shower width, and the test data show that electron showers have $\sigma < $ 11cm (for 80% containment) for all electron energies of interest in the experiment (Fig. 19.).

The requirement of these values for Γ and σ in the electron definition allows a separation of electron and pion showers with a rejection of the π showers by a factor larger than 100 and a global electron efficiency $\varepsilon_{el} = 0.6$ for the case where all types of electron showers are considered ($3 \leq E_F \leq 50$ MeV). Further separation can be obtained by counting the number of holes in the streamer-tube hit distribution in the first eight radiation lengths of a shower. The efficiency in selecting electron and pion showers by requiring a minimum energy-dependent number of holes (referred to as "holicity") is shown in Figure 20.

Figure 19: Values of Γ and σ for Electrons and Pions
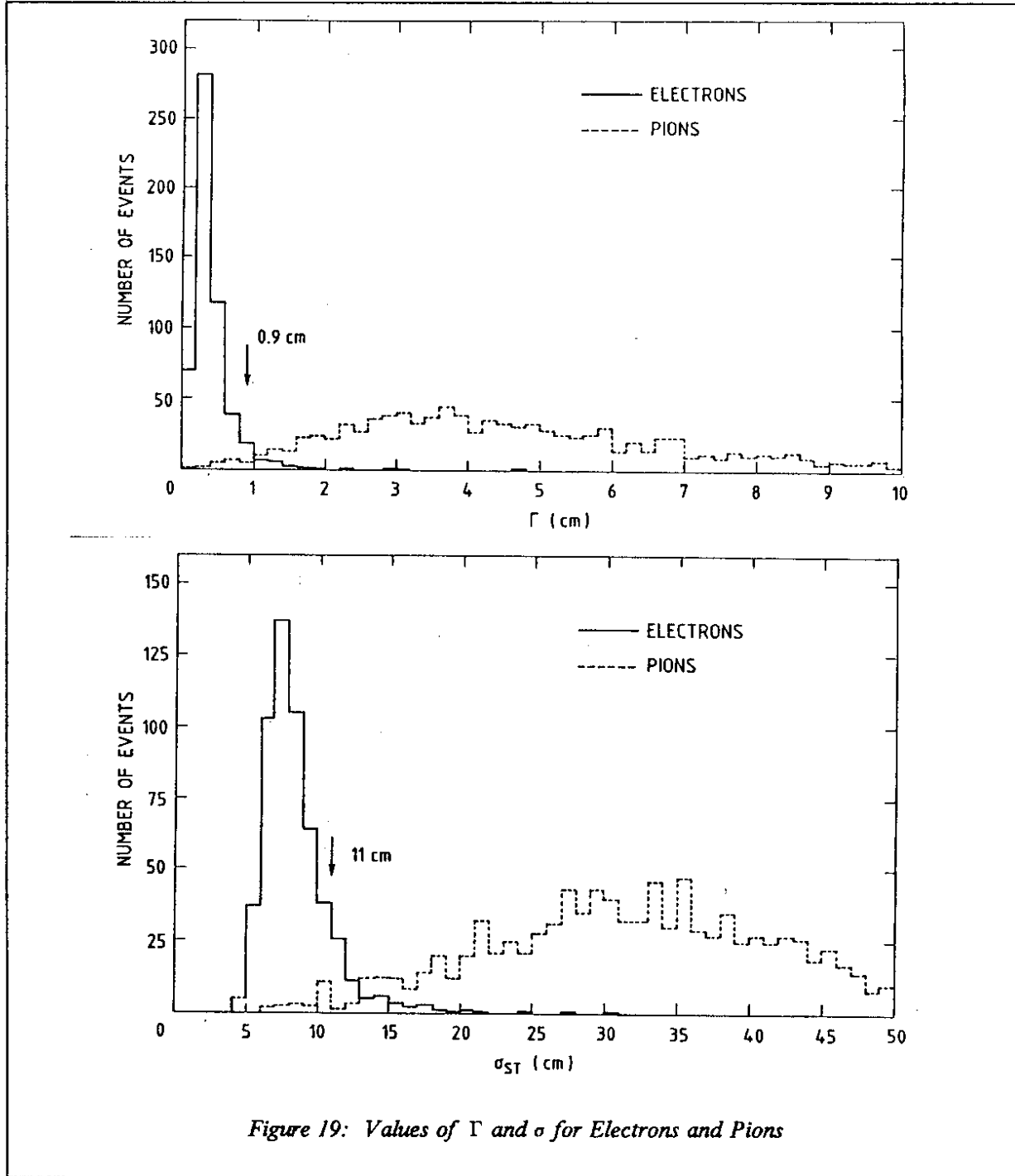
3.6 Measurement of Electromagnetic Showers Embedded in Hadronic Cascades

The fine granularity of the CHARM calorimeter allowed electromagnetic showers originating at the interaction vertex to be identified even in the presence of hadronic showers for part of the kinematic y-range of ν_e-interactions. Since the CHARM detector was designed to equalize the average length of hadronic and electromagnetic showers [1], the length could not be used directly to discriminate electromagnetic and hadronic showers. However, electromagnetic showers are much narrower and

Figure 20: Efficiency of Selection of Electrons and Pions by Holicity
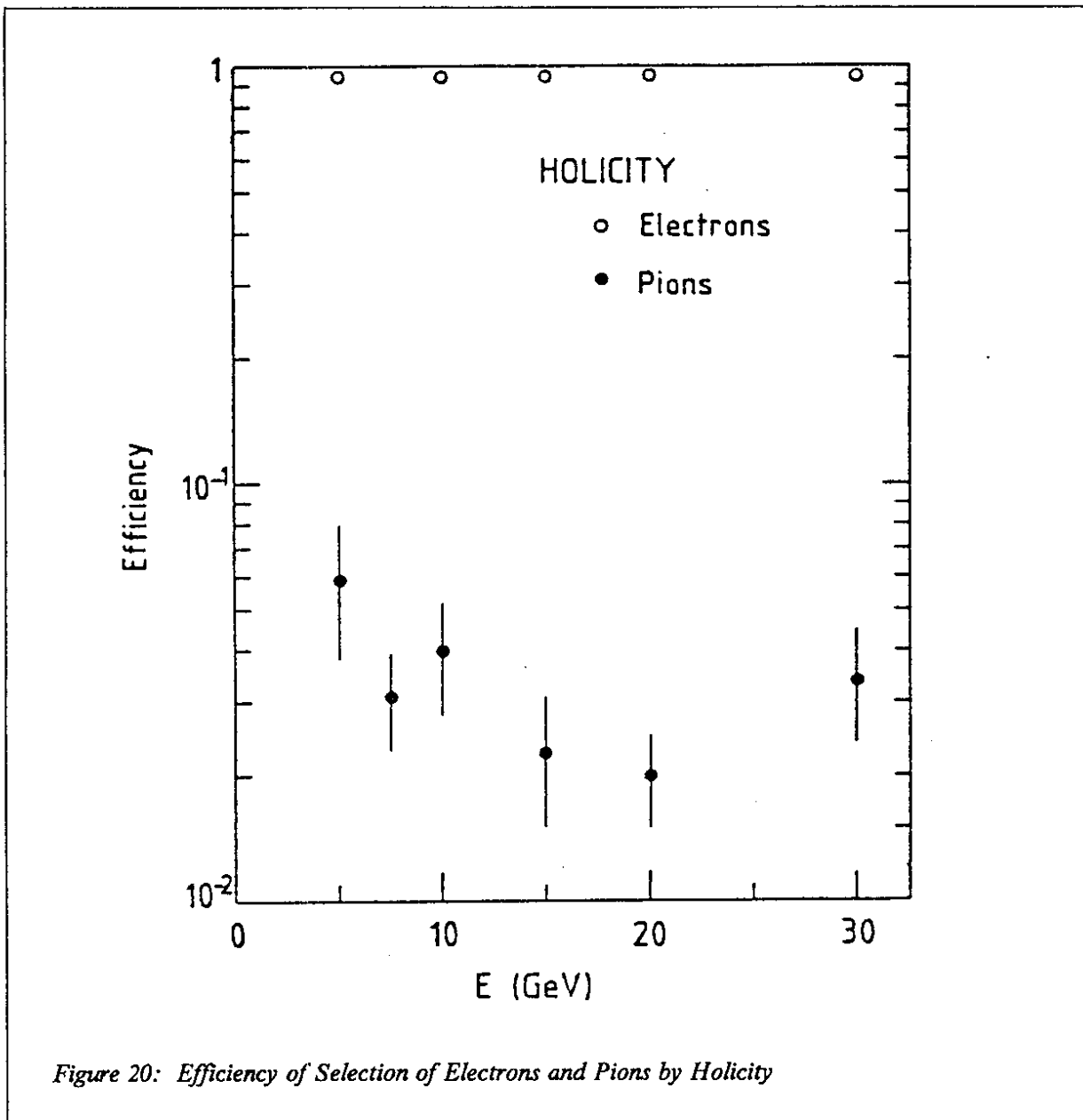
much more regular in their longitudinal development than those originating from hadrons. The procedure used these two characteristic differences, in a somewhat different way to that described in the previous section.

The input to the electron search program was the energy as measured in the scintillation counters. A very restricted volume was used in this search for electromagnetic showers. A road was defined starting at the position of the reconstructed interaction vertex whose length was chosen according to the energy of the electron candidate, which was determined from the test beam data to be typically to be 3/4 of the full shower length to obtain 95% containment. The width of the road corresponded to the width of the scintillator elements. The typical width of an electron shower in the calorimeter was 2.5 cm FWHM as compared to the scintillator width of 15 cm.

A direct separation of electron-neutrino induced charged-current events from all muonless events was performed by computer code. The method was used in the beam dump experiment [8]. In the case of ν_e and $\bar{\nu}_e$ induced charged-current events the shower detected in the calorimeter consisted of two components, an electromagnetic part induced by the electron, and a hadronic part induced by the recoiling hadron system. In most cases these two components were not separated in space.

Four different estimators were used to determine the energy of electron candidates. They were based on the energy detected:

1. in the scintillator at the maximum of the shower development;

2. in three scintillators around and including the shower maximum in 3 adjacent planes, combining information of scintillators of horizontal and vertical orientation;

3. in all horizontally oriented scintillators of the road;

4. in all vertically oriented scintillators of the road.

These estimators were strongly correlated for electromagnetic showers.

The search was performed for a large number of trials for the shower direction starting at or in the vicinity of the reconstructed interaction vertex. The most probable candidate for an electromagnetic shower was taken from the trial for which the energy estimators showed the best consistency with the data taken in the test beam using incident electrons.

A demonstration of the power of these estimators is shown in Figure 21, where the electron search algorithm has been applied to 15 GeV test beam data for both electrons (full histogram) and pions (dashed histogram). The inelasticity y defined as

$$y = (E_{total} - E_{electromagnetic})/E_{total}$$

is shown, where $E_{electromagnetic}$ is obtained from the weighted average of the four energy measurements. The resolution and response of the estimators were calibrated with data recorded in the test beam for energies from 5 GeV to 50 GeV. Showers generated by Monte Carlo simulation were used to extend the calibration range up to 150 GeV.

For charged current (CC) ν_e ($\bar{\nu}_e$) events the response of the estimators is shifted and the resolution deteriorated by the presence of the hadronic shower in the volume of the search. This effect was evaluated by applying the method to semi-Monte Carlo events, which were constructed by using CC ν_μ-events recorded in a neutrino exposure, for which the muon was replaced by an electromagnetic shower of the same energy and direction generated by a Monte Carlo program.

Applying this method to events which do not contain an electron from charged-current ν_e (or $\bar{\nu}_e$) interactions also leads to an estimate of the electromagnetic content of the hadronic showers. Such events contribute to the background.The shape of this background distribution was determined by applying the method to a data sample collected in the wide-band beam which contains only a small contamination of electron neutrinos which was taken into account. The resulting y-distribution for a data sample from a beam-dump exposure is shown in Figure 22. The figure illustrates a fit for events in the energy range $40-60$ GeV using data taken during a beam dump experiment. a) shows the measured y-distribution (full line) and the background component (dashed line), b) shows the background subtracted y-distribution (full line) and the Monte Carlo prediction (dashed line).
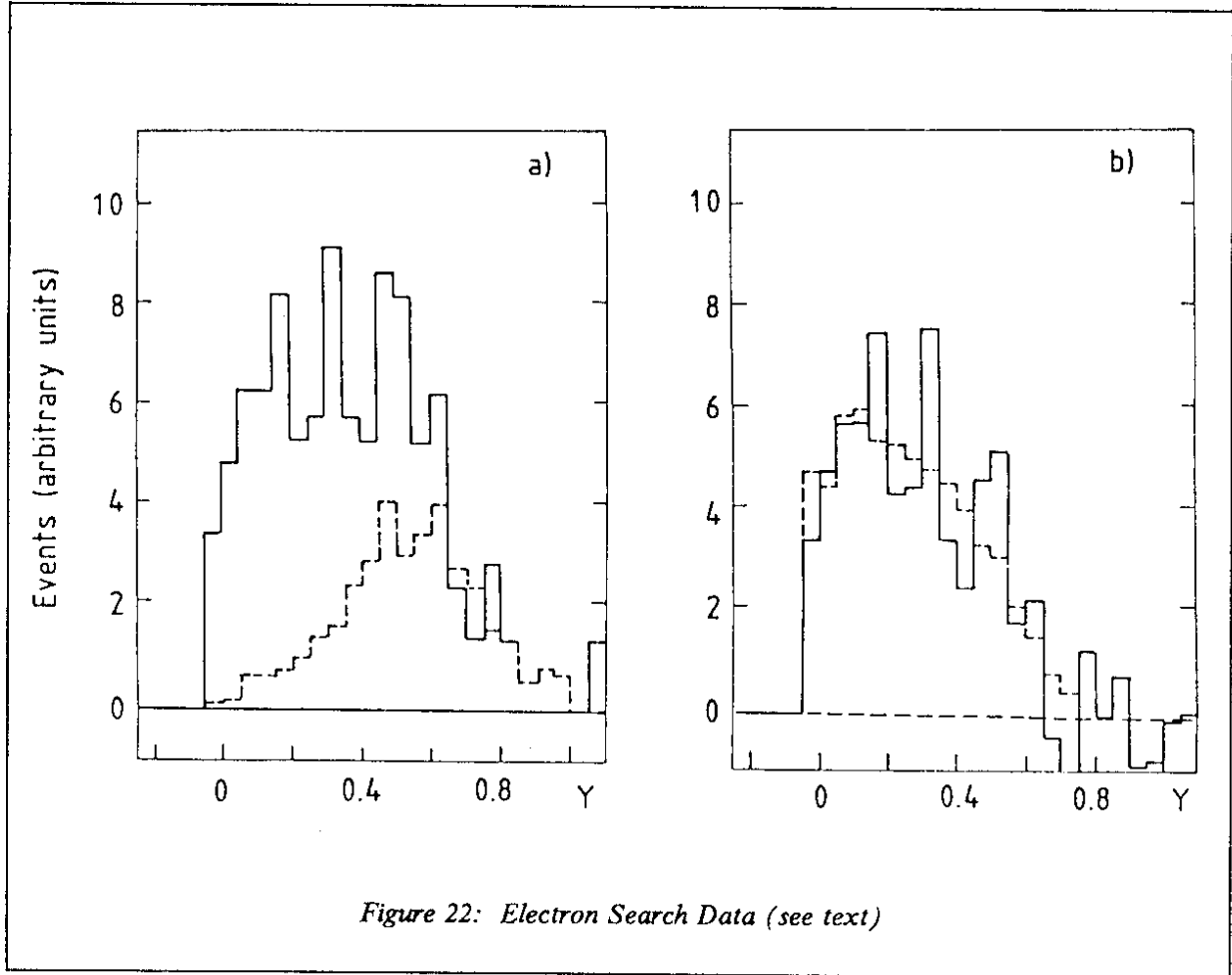
Figure 21: Electron Search Algorithm on 15 GeV Data
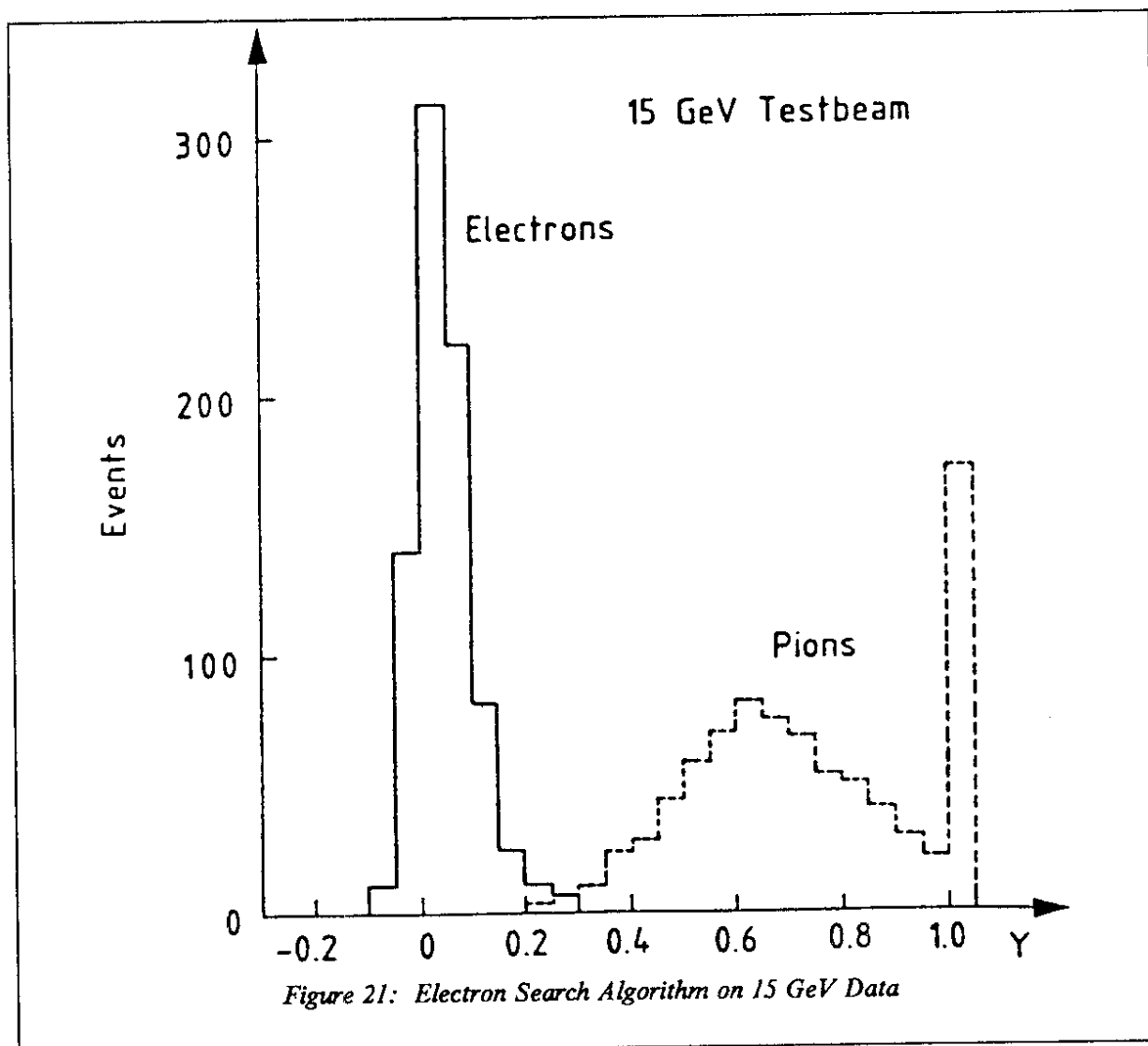
Figure 22: Electron Search Data (see text)

4. Conclusions

The CHARM calorimeter has been used extensively for the study of neutrino interactions over a period of seven years. The need for detailed calibration of the response of this detector has been explained in section 1.2. As a result of measurements made in a test beam over the energy range 5-140 GeV, the response of the calorimeter to both pions and electrons has been fully explored.

Specific results obtained are:

- Energy response and resolution for hadronic showers
- Energy response and resolution for electromagnetic showers
- Angular resolution of both hadronic and electromagnetic showers
- Identification of electromagnetic showers from the shower shape
- Measurement of electromagnetic showers embedded in hadronic cascades

These results have also led to an understanding of the showers produced by electron-neutrino induced interactions, which can contain both hadronic and electromagnetic components, from which the kinematic parameters relevant for the neutrino physics could be obtained.

5. Acknowledgements

References

[1]   A.N.Diddens, M.Jonker, J.Panman, F.Udo, J.V.Allaby, U.Amaldi, G.Barbiellini, A.Baroncelli, V.Blobel, G.Cocconi, W.Flegel, W.Kozanecki, E.Longo, K.H.Mess, M.Metcalf, J.Meyer, R.S.Orr, F.Schneider, A.M.Wetherell, K.Winter, F.W.Büsser, P.D.Gall, H.Grote, P.Heine, B.Kröger, F.Niebergall, K.H.Ranitzsch, P.Stähelin, V.Gemanov, E.Grigoriev, V.Kaftanov, V.Khovansky, A.Rosanov, R.Biancastelli, B.Borgia, C.Bosio, A.Capone, F.Ferroni, P.Monacelli, F.de Notaristefani, P.Pistilli, C.Santoni and V.Valente, CHARM Collaboration; "A Detector for Neutral-Current Interactions of High-Energy Neutrinos", Nucl. Instr. and Meth. 178 (1980) 27.

[2]   M.Jonker, J.Panman, F.Udo, J.V.Allaby, U.Amaldi, G.Barbiellini, A.Baroncelli, V.Blobel, W.Flegel, W.Kozanecki, K.H.Mess, M.Metcalf, J.Meyer, R.S.Orr, F.Schneider, A M.Wetherell, K.Winter, J.Aspiazu, F.W.Büsser, P.D.Gall, H.Grote, B.Kröger, E.Metz, F.Niebergall, K.H.Ranitzsch, P.Stähelin, P.Gorbunov, E.Grigoriev, V.Kaftanov, V.Khovansky, A.Rosanov, B.Borgia, C.Bosio, A.Capone, F.Ferroni, E.Longo, P.Monacelli, F.de Notaristefani, P.Pistilli, C.Santoni and V.Valente, CHARM Collaboration; "The Response and Resolution of a Fine-Grain Marble Calorimeter for Hadronic and Electromagnetic Showers", Nucl. Instr. and Meth. 200 (1982) 183.

[3]   M.Jonker, F.Udo, U.Amaldi, R.Donnet, W.Flegel, B.Friend, E.Gygi, M.Jimenez, A.King, F.Schneider, V.Valente, A.M.Wetherell, F.Niebergall, J.Schütt, and D.De Pedis; "Use of Streamer Tubes in a Large Calorimetric Neutrino Detector", Physica Scripta 23 (1981) 677.

[4]   M.Jonker, F.Udo, U.Amaldi, R.Donnet, W.Flegel, B.Friend, E.Gygi, M.Jimenez, A.King, F.Schneider, A.M.Wetherell, J.Aspiazu, F.Niebergall, J.Schütt, F.Ferroni, D.De Pedis and V.Valente; "The Limited Streamer Tube System of the CHARM Collaboration", Nucl. Instr. and Meth. 215 (1983) 361.

[5]   I.Abt, H.Daumann, P.Stähelin, P.Gorbunov, L.Luminari, W.Flegel, M.Metcalf, R.S.Orr and J.Panman; "Pattern Recognition for Hadronic Showers in the CHARM Calorimeter", Nucl. Instr. and Meth. 217 (1983) 377.

[6]   G.Battistoni, E.Iarocci, G.Nicoletti and L.Trasatti; "Detection of Induced Pulses in Proportional Wire Devices with Resistive Cathodes", Nucl. Instr. and Meth. 152 (1978) 423.

[7]   P.A.Gorbunov, E.A.Grigoriev, V.A.Gemanov, V.A.Zaitsev, S.A.Zeldovitch, V.S.Kaftanov, Yu.G.Kornelyuk, M.A.Kubantsev, A.M.Maslennikov, A.N.Rosanov, M.S.Ryabinin, M.M.Savitsky, V.M.Serejin, V.D.Khovansky and V.Sh.Epstein, Institute for Theoretical and Experimental Physics, Moscow; "Calibration of a Fine-Grained Calorimeter with Beams of Hadrons and Electrons in the Momentum Range 0.5 - 6 GeV/c", Preprints ITEP-38 and ITEP-53 (in Russian).

[8]   M.Jonker, J.Panman, F.Udo, J.V.Allaby, U.Amaldi, G.Barbiellini, A.Baroncelli, V.Blobel, W.Flegel, W.Kozanecki, K.H.Mess, M.Metcalf, J.Meyer, R.S.Orr, F.Schneider, V.Valente, A.M.Wetherell, K.Winter, F.W.Büsser, P.D.Gall, H.Grote, B.Kröger, E.Metz, F.Niebergall, K.H.Ranitzsch, P.Stähelin, P.Gorbunov, E.Grigoriev, V.Kaftanov, V.Khovansky, A.Rosanov, R.Biancastelli, B.Borgia, C.Bosio, A.Capone, F.Ferroni, E.Longo, P.Monacelli, F.de Notaristefani, P.Pistilli, and C.Santoni, CHARM Collaboration; "Experimental Study of Prompt Neutrino Production in 400 GeV Proton-Nucleus Collisions", Physics Lett. 96B (1980) 435.